Evaluation of a Reluctance Synchronous Motor

For use in a Mine Shuttle Traction Vehicle

Mikail Muhammad Aleem Ansari

A Dissertation submitted to the Faculty of Engineering and the Built Environment, University of the Witwatersrand, in fulfilment of the requirements for the degree of Master of Science in Engineering.

Johannesburg, 2011

Declaration

I declare that this dissertation is my own unaided work. It is being submitted for the Degree of Master of Science to the University of the Witwatersrand, Johannesburg. It has not been submitted before for any degree or examination to any other University.

....
(Signature of Candidate)

.... day of .... year ....
day *month* *year*

ABSTRACT

Electric motors play an important role in modern societies, and have many applications from causing mobile phone vibration to steering space shuttles. While many industrial applications use the Induction Motor (IM), this motor has the potential to be improved upon by the Reluctance Synchronous Motor (RSM) in specific niche applications like Mine Shuttle Vehicles (MSV). The possibility of these improvements led to a mine shuttle IM's manufacturer to partner with the University of the Witwatersrand to study the improvements that the RSM can offer. A prototype RSM was designed and built, and needed to be tested to assess these improvements.

The RSM was compared with the IM on the following parameters: torque production for the MSV, construction quality and cost of construction. A manufacturing advantage of the RSM is that it can be converted from an IM cheaply and offers greater torque. This prototype RSM was able to produce 3.6% more torque than the IM at the same levels of current. Furthermore due to its improved construction, more current can be supplied to the RSM which allows it to generate 43% more torque. These measurements proved that the RSM is a viable alternative to the IM in the MSV as it provides a higher torque density. While the results show that the IM is still highly efficient, the RSM does improve upon it slightly, in niche applications like the MSV. These results justify future research on the RSM's efficiency.

In the name of Allah, the most kind the most merciful

> “So, verily, with every difficulty, there is relief: (5)
> Verily with every difficulty there is relief. (6)”
>
> The Holy Quran (Surah 94, Ayahs 5:6)

ACKNOWLEDGEMENTS

I would like to thank Allah (S.W.T.) for the opportunity to research the Reluctance Synchronous Motor, for gifting me with awesome parents, for providing me with a good supervisor, helpful professors, and nice colleagues in the Future Electrical Energy Technology research group at the University of the Witwatersrand.

I would also like to thank:

My supervisor Prof. W. A. Cronje for his guidance

Mr A. Meyer and Prof. I. Hofsajer for their advice

Mr H. Fellows, Mr D. Fellows, Mr M. Goosen, Mr A Mkwanazi, Mr F. Sithole, my fellow postgraduate students and the Writing Centre for their assistance

Mr M. Pardini and Mr S. Pardini at Transvaal Electric (Pty) Ltd for the project support

The University of the Witwatersrand, for the opportunity to explore

Mikail Muhammad Aleem Ansari

Johannesburg, 2011

Contents

Chapter 1

INTRODUCTION

Electric motors and machines play an important role in society. This is evident in the wide variety of applications that they have in devices ranging from mobile phones, computers, lawn mowers, pool pumps and space shuttles [1] to modern cars having more than 50 electric motors [2] (windshield wipers, electric windows and so forth). Despite the pervasive presence of electric motors, they can still be improved to reduce manufacturing costs and optimise energy efficiency for niche applications.

1.1 ENERGY USAGE OF MOTORS

Improving motors is important due to their contribution to overall energy usage. The International Energy Agency (IEA) estimates that motors contribute the largest portion of global electrical energy demand (EED) [3], Figure 1.1a.

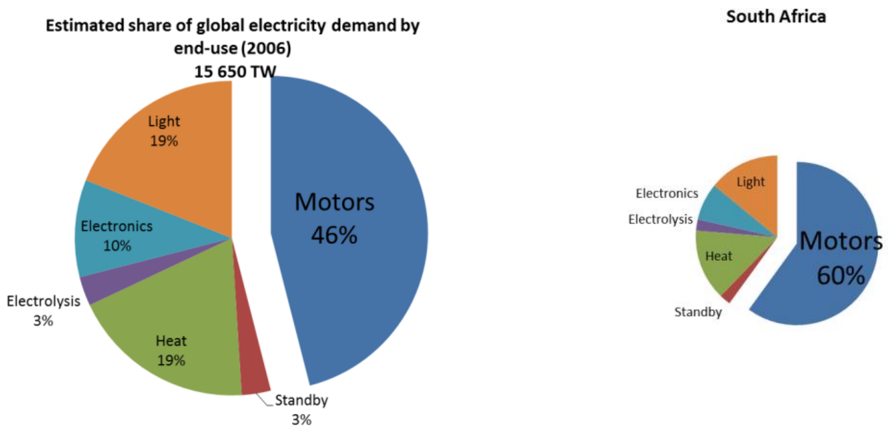

a. b.

Figure 1.1: Estimated electricity demand a) Globally [3], and in b) South Africa [4] (not to scale)

Electric motor EED in South Africa is even higher than global averages where approximately 60% of South Africa's total EED is due to powering electric motors, Figure 1.1b [4].

The statistics highlight that reducing energy usage in the world and within South Africa relies on improving existing motors. To improve upon these motors and reduce EED, it is important to break these statistics down to determine:

- What types of motors are responsible for the majority of energy usage?
- What are the sizes of these motors?
- Which sectors of society use the most number of motors?

1.2 Types of motors

There are many different types of motors, however the Induction Motor (IM) contributes to the majority of motor sales [5]. In the European Union (E.U.) motor sales are dominated by 3-Phase AC Induction Motors (Figure 1.2).

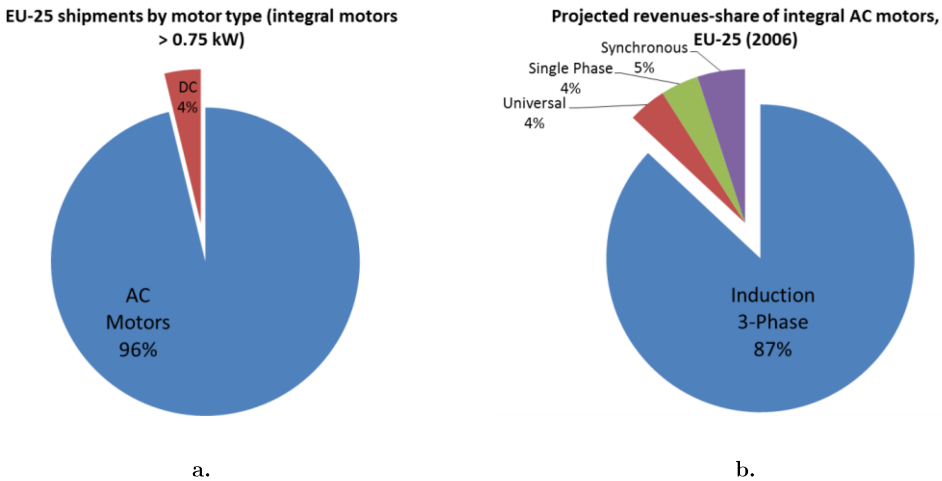

Figure 1.2: The E.U. Motor market (for integral motors) in 2006 a) All motors, and b) AC motors [5]

This is mainly because of the IM's:

- Lower Cost (Material requirements and complexity)
- Robust construction
- Versatility

Due to its prevalence, the Induction Motor is used as a benchmark for evaluating other motors. A comparison of the properties of industrial motors is shown in Table 1.1. The Reluctance Synchronous Motor (RSM) compares favourably to other motors, particularly at higher torque levels. This shows that the RSM has the potential to offer greater efficiency than the IM at a lower cost [6].

Table 1.1: Properties of different types of motors.

Motor Type	Torque Density	Cost	Flux weakening	Cold Rotor
Reluctance Synchronous	+	+	+	+
Brushless (rare-earth)	+	-	-	+
Brushless (ferrite)	-	+	-	+
Induction (field oriented)	-	+	+	-

Further analysis, of motor sizes and the sectors of society that use the most number of motors, is shown in Figure 1.3.

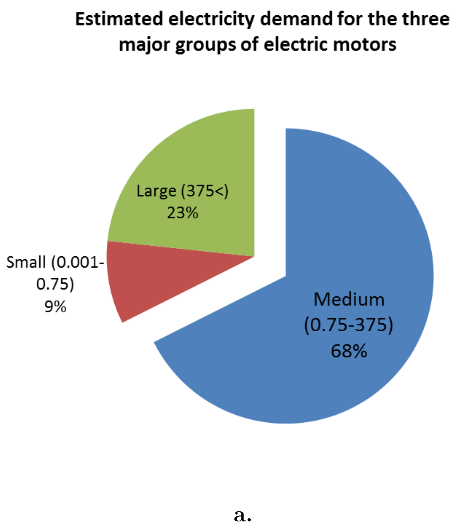

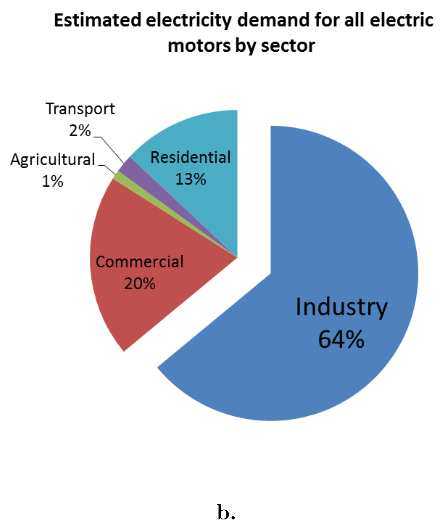

Figure 1.3: Global electricity demand from motors a) by motor size (kW), and b) by sector [3]

The breakdown of these statistics shows that:

- 3-Phase AC Induction Motors are the most prevalent
- Motors sized between 0.75 and 375 kW[1] are responsible for the majority of EED, Figure 1.3a
- Industry uses the largest number of motors, Figure 1.3b

These statistics show that to reduce global electrical energy demand, research into improving upon the 3-phase induction motors is important. The research was based on a mine shuttle vehicle application as it fits into all the major categories discussed (AC Motors, Induction Motors, 3-phase, between 7.5 to 375kW).

1.3 Mine shuttle

The electric motor research and evaluation used the mine shuttle vehicle as an application to study [7]. This was because the traction for the mine shuttle is provided by 3-phase 55 kW AC induction motors, which fit into the categories mentioned above. The manufacturer for this Induction Motor wanted to be able to provide a motor for the same application but produce it more cheaply whilst offering the same performance. In order to optimise performance, analysis of the application is required.

Looking at the mine-shuttle system as a whole is important as research [3] has shown that while improvements to individual motors are tough to achieve, vast improvements can be made when considering the motor in terms of the overall application and the total system's efficiency.

---

[1] The larger motors contribute to higher energy demand even though smaller motors sell more units.

[2] The reason that a variable transformer (Variac) could not be used is that the Variac

The mine shuttle is a vehicle used in the mining industry, all over the world, to transport a variety of materials within the harsh environment of a mine. The mine shuttle is a rugged vehicle specifically suited to this environment. Cool air is a vital commodity underground where dust particles and rocks can often impede the path of shuttle vehicles. To overcome these obstacles, a large amount of thrust is required.

1.3.1 Generating thrust

Conventional vehicles generate thrust by using an internal combustion engine (ICE). Combustion engines emit pollutants and in an open air environment, this does not present a large issue. However in an underground environment such as mines, this can become hazardous. This is why mine shuttle vehicles currently use Induction Motors (IM) to generate torque.

In order to adjust the torque and the speed, a Variable Speed Drive (VSD) is used. The VSD electronically generates a varying sinusoidal signal that powers the motor. As the mine shuttle already uses a VSD, the IM can be replaced by a RSM (which requires a VSD to operate). The RSM is expected to offer increased efficiency at a reduced cost. The RSM has advantages such as robust construction [8,9], lower manufacturing costs, easier control implementation, synchronous speed operation, "cold" rotor capability (reduced heat losses) and the capability of high speed applications. Further details of the RSM and VSDs are presented in later chapters.

The mine shuttle IM's manufacturer is interested in the RSM as it has the potential to improve upon the IM in the following key areas:

- Improving torque density, greater torque within the same frame size.

- Reducing weight and inertia, which would improve mechanical performance.
- Reducing heat-losses, which should extend the lifetime of the motor, reduce motor burn-outs, and increase robustness.
- Reduce material (copper bars) requirements, which reduces costs.
- Reducing the complexity of the manufacturing process, as simplifying manufacturing will further reduce costs.

1.4 Prior work

Based on the possibility of these improvements, an RSM prototype was initially designed (using Finite Element Modelling - FEM) in the previous research [10] and built. This research seeks to confirm the improvements that the RSM can provide, by validating the values that were predicted in the initial design simulations.

1.5 Problem statement

*The **Reluctance Synchronous Motor (RSM)** has the **potential** to improve upon the existing **Induction Motor (IM)**. In order to **verify** these improvements in a **mine-shuttle vehicle**, a **prototype RSM** has been **designed*** [10] *and **built**. **Both** motors need to be **evaluated** to validate the improvements, in terms of construction **costs**, **quality** and **performance**.*

1.6 Aim of the study

The aim of the study is to validate the initial design [10] by confirming the predictions made through simulations. This will be done by evaluating and testing both the Induction Motor and Reluctance Synchronous Motor. The characteristics for this evaluation are:

- Construction and manufacturing of the motors
- Torque production of the motors

The eventual application of the motor in a mine-shuttle vehicle will be considered when evaluating these characteristics.

1.7 Organisation of this Dissertation

In this dissertation:

- Details about the manufacturing and construction of the IM and the RSM are presented first.
- Then: the experimental setup of both motors, details of the various experiments and their results are presented.
- Lastly, the analysis and the findings are presented.

1.8 Summary

This chapter provided an introduction to the research that has been conducted and describes why there is a need for Reluctance Synchronous Motors. The aim of the research was introduced and it was emphasised that the two different types of motors will be evaluated, in order to determine the advantages and disadvantages associated with each motor. The mine shuttle application and the environment in which the motor operates were examined. The theoretical advantages of the Reluctance Synchronous Motors were also presented.

The following chapters will describe the construction of the two motors, the experiments performed on these motors and lastly, the analysis of which motor presents the most cost effective performance is presented.

Chapter 2

Motors

The first chapter introduced the field of research and discussed why the Reluctance Synchronous Motor (RSM) is thought to be better suited to the mine shuttle application than the Induction Motor (IM). The IM was dominant in the industrial sector because of its cheaper and robust construction. Due to the importance of the cost and quality of construction, this chapter delves further into the manufacturing processes and operation of the Induction Motor (IM) and the Reluctance Synchronous Motor (RSM).

2.1 Induction Motor

The squirrel cage IM's construction and operation is well known, and is summarised below.

2.1.1 Construction

The squirrel cage IM that is currently used in the mine shuttle vehicle is shown in Figure 2.1 (adapted from [11]). The IM construction is subdivided into two main components, namely the rotor (rotating part of the motor) and the stator (stationary part of the motor).

The stator consists of a number of thin laminations that are stacked together. Coils of wire are then wound along this stator stack in a distinct pattern. The rotor also consists of these thin laminations which are stacked together. The squirrel-cage rotor configuration consists of thick aluminium/copper bars that are embedded into the stack, Figure 2.1.

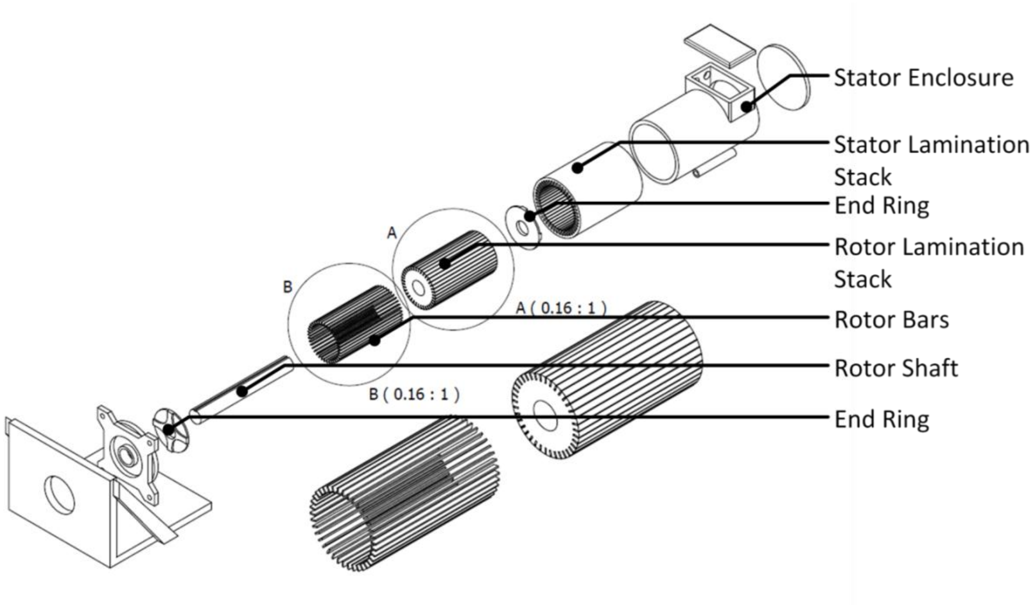

Figure 2.1: Construction of a Squirrel Cage Induction Motor

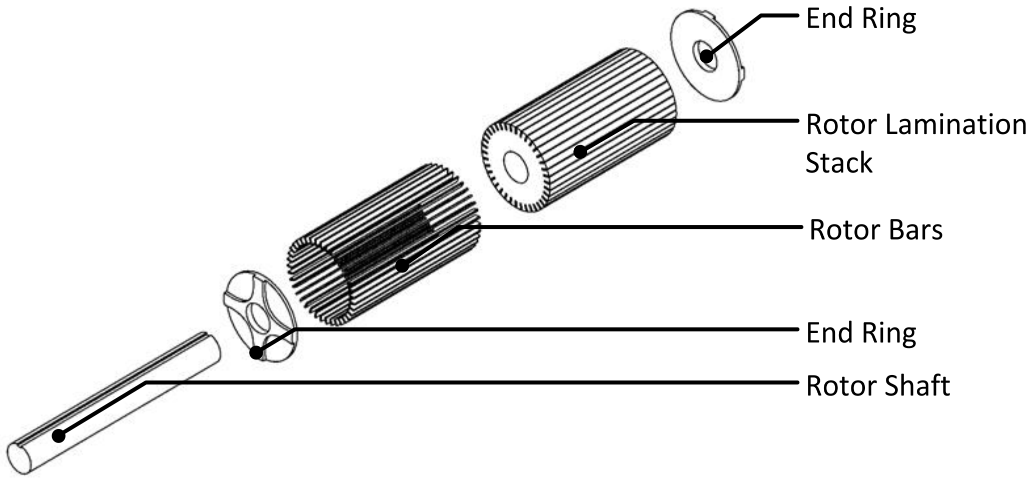

Figure 2.2: Rotor of an Induction Motor

2.1.2 Operation

The coils within the stator help to establish a magnetic field, and also induce currents within the rotor bars. The currents in the bars establish their own magnetic field which opposes the field established by the stator winding.

As both fields oppose each other, the rotor (which is free to move because of mechanical bearings) rotates to reduce the effect of this opposing field. Due to the sinusoidal current that flows in the stator windings, this magnetic field constantly "follows" the rotor to keep the rotor moving.

2.1.3 Analysis

The simple and versatile construction of the IM, when compared with other motors, is what has led to it dominating the market segment. The embedded rotor bars allow the motor to be "plugged directly into mains" and automatically start up, are the primary components that help to generate torque.

However, some disadvantages that these bars introduce can be improved upon by other motor designs, such as:

- Costs, in terms of:
  - The additional materials (copper) required in producing the bars.
  - Manufacturing complexity, of having to embed the bars into the rotor as well as cutting the rotor stack into smaller laminations to constrain the current to flow along these bars.
- Construction Quality/Robustness
  - The end rings introduce extra welds within the motor which could be more susceptible to failure.
- Efficiency
  - The heat and resistive losses within the rotor. These losses are due to the current that is carried in the bars, which heats up the bars as a result of eddy currents. In temperature sensitive environments like mines, where a lot of effort is placed in cooling systems, it is unreasonable to have a motor that heats up during operation. These problems are exacerbated if an obstacle impedes the path of the mine shuttle, which can cause the motor to heat up even more, when trying to overcome those

obstacles. An overheating motor is a great concern in environments which need to be kept cool, such as underground mines. The IM is highly efficient. However the torque of an Induction Motor cannot be increased above rated torque without losing its efficiency. This is because the larger amount of current causes greater heat loss.

A motor that heats up due to performance losses is an issue that is further exacerbated in underground mines. Motors that have reduced heating effects would be better suited to these environments. The environments in which the mine shuttle vehicle operates require an alternative to the IM. As IM within the shuttle vehicle already uses a VSD, a motor like the RSM can be considered. The RSM has the potential to offer a cheaper construction and reduced losses.

2.2 Reluctance Synchronous Motor

The theory for Reluctance Synchronous Motors (RSMs) has been available since 1918 [12,13,14], however the wide scale adoption of this motor in industry has been limited [6]. This is because it cannot be satisfactorily operated directly from the mains supply/power utility [6].

Recent advances in power electronics and the development of variable speed drives (VSDs) for Induction Motors have made it possible to design RSMs for commercial applications that already use VSDs. These developments led to the design of a new RSM to research its feasibility in providing traction for a mine shuttle. This RSM was designed at the University of the Witwatersrand together with an industrial partner [7].

2.2.1 Construction

The prototype RSM uses the same stator as the original IM. This reduces costs and limits component remanufacturing. It also shows the economic and efficiency advantages of converting an existing motor as opposed to completely replacing the motor. Furthermore when looking at the RSM from a production standpoint the assembly line for the IM stator can still be maintained and only the rotor assembly process will need to be changed.

The RSM rotor is constructed differently to that of the IM. The rotor is cut out in a very distinct pattern. The pattern creates a varying reluctance by incorporating the air gaps (which are very reluctant to magnetic fields) and magnetic material (which has reduced reluctance). The pattern removes the need for bars in the rotor. The construction of the RSM rotor is shown in Figure 2.3. A cross-sectional view of the designed RSM pattern is shown in Figure 2.4 (adapted from [9]).

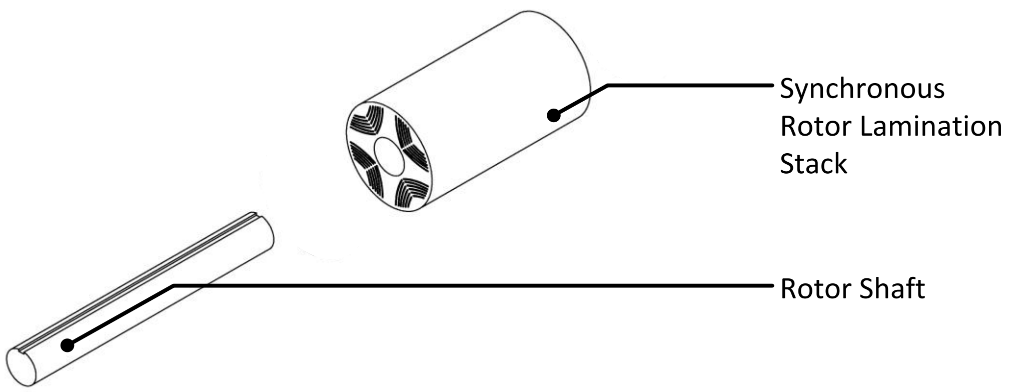

Figure 2.3: Reluctance Synchronous Motor Construction

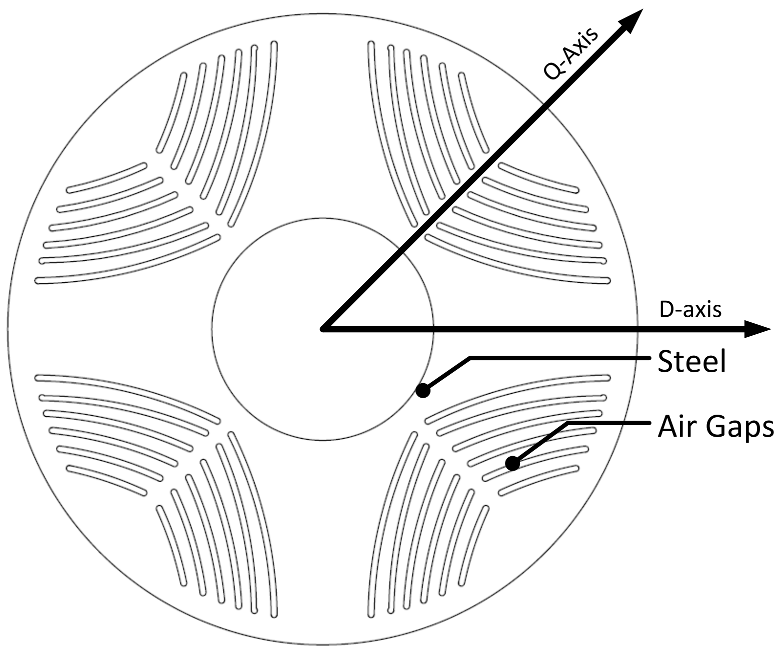

Figure 2.4: Reluctance Synchronous Motor Designed at the University of the Witwatersrand [9]

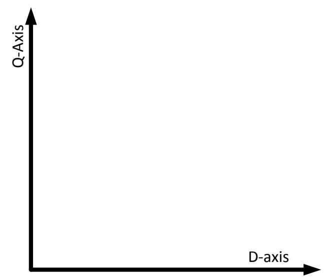

Figure 2.5: Vector diagram of the RSM's d-q axis in (electrical degrees)

The d-q (direct and quadrature) axes shown in Figure 2.4 represent the axes in the mechanical reference frame. An important point to note is the difference between electrical and mechanical rotor degrees. The d-q axes are, by definition 90 electrical degrees apart, Figure 2.5. The d-q axes in the rotor being tested are 45 mechanical degrees apart. In order to change between the electrical and physical reference frames, a scaling factor of two needs to be incorporated.

2.2.2 Operation

The RSM works on a different principle to that of the IM. It uses the principle magnetic reluctance to generate torque, that certain materials are more “reluctant” to magnetic fields than others. The least reluctant path will try to align with the magnetic fields setup by the travelling wave.

This is similar to the way in which a switched reluctance motor operates however the RSM has the advantage of being able to operate synchronously using the 3-phase resultant vector thereby reducing torque ripple.

2.2.3 Analysis

The RSM design offers several advantages over the traditional IM.

- Firstly, it does not require the rotor bars to operate, thereby reducing
  - Resistance and heat losses [15] associated within the rotor.
  - Assembly and copper costs.
  - Weight of the rotor, which reduces the inertia
- Secondly, as the rotor does not carry any eddy currents (as a time varying field is not present), the rotor does not have to be sliced into very thin laminations. This further reduces the manufacturing costs.
- It allows for higher torque to be produced.
- Lastly, the motor can achieve higher speed operation, using flux weakening [6].

As the RSM construction uses the same stator as the IM, an IM can be converted in to an RSM by simply changing the rotor. This further saves costs while optimising efficiency.

The disadvantage of the RSM relates to its versatility. As it cannot be directly plugged in and started from the mains supply, and requires a variable frequency supply in order to operate.

However the effect of this disadvantage is lessened, as many modern industrial applications already use Variable Speed Drives (VSDs) and the cost of VSDs continues to decline. Furthermore, the RSM's varying reluctance construction is better suited to these VSD applications.

2.3 Variable Frequency/Speed Drives (VFD/VSD)

Variable Speed Drives (VSDs) are well known in the motor industry and are briefly discussed below.

2.3.1 Background

Historically industrial motors have been designed for fixed speed systems so that they achieve maximum output when connected to the grid/power utility input. As the power supply has always had a fixed frequency, the motors have to run at constant speed. The speed of industrial motors had to be initially adjusted by increasing the loading:

> An example of this is an industrial fan. The fan motor would always run at maximum speed, and a variable output would be achieved by controlling the vents. If all the vents are open it would result in maximum output, if some vents were closed it would result in a reduced output. However, this is a highly inefficient way of using power as the motor runs at maximum power regardless of usage. It sometimes even results in increased loading of the motor, as it faces greater air resistance in trying to push the air through reduced number of vents.

Many industrial applications such as fans, pumps, air-conditioners and electric vehicles require variable speed control. Due to the increased cost of electricity and heightened environmental concerns, it has become more and more important to achieve efficient speed control. A cost effective way of speed control has not be available until recently.

Advancements in power electronics, semiconductor manufacturing, microprocessors and control theory components have allowed Variable Speed Drives to be built cheaply and become commercially viable. These drives generate electronic signals of varying width which approximate to a sinusoidal signal from the grid, which is required by motors.

2.3.2 Construction and Operation

VFDs or VSDs use electronic switches (transistors) to create pulses of voltage on the output. The width of these pulses can be controlled by accurately timing the switching operation. This process is known as Pulse Width Modulation (PWM). By using accurate PWM, different types of signals can be generated. This process is shown in Figure 2.6.

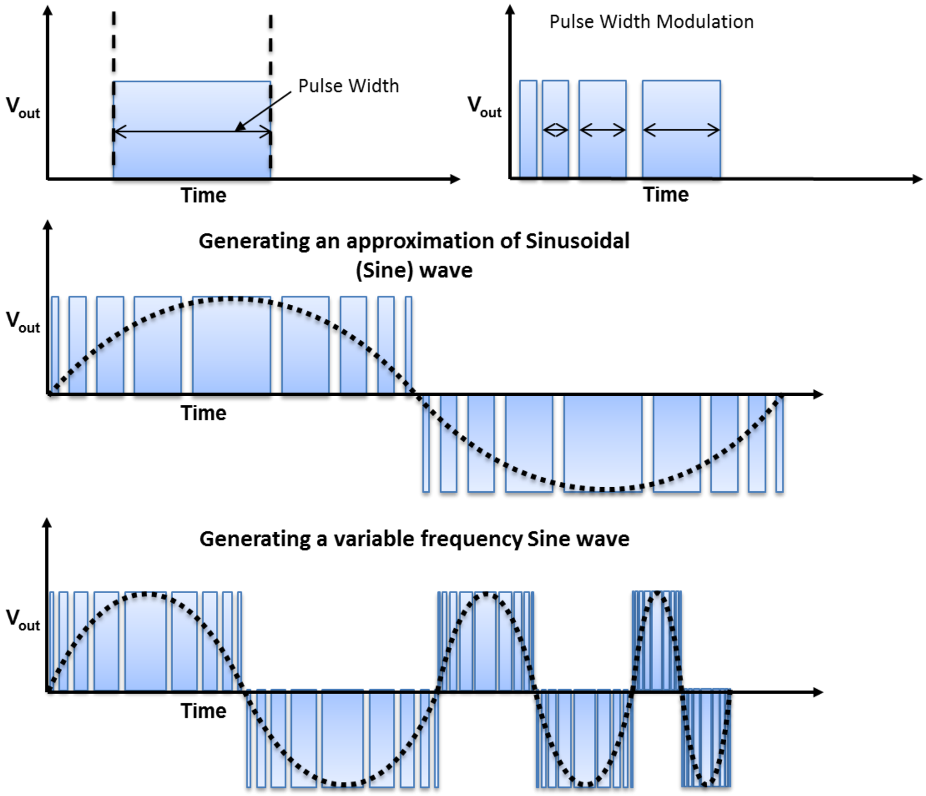

Figure 2.6: Variable Frequency/ Speed Drives

2.4 Summary

This chapter provided details of the manufacturing processes and the operating principles of the Induction Motor (IM) and the Reluctance Synchronous Motor (RSM). The advantages and disadvantages of the motors were analysed and showed that the RSMs are better suited to variable speed applications. Variable Speed Drives (VSDs) were also discussed briefly. The next chapter deals with the experimental setup, measurement and results which are necessary to accurately grade the improvements that the RSM provides.

Chapter 3

Motor Testing

The manufacturing processes and construction details of the two motors were discussed in the previous chapter. This chapter deals with the experimental testing for both motors.

3.1 Apparatus

In order to test the two motors, specialised equipment was required.

3.1.1 Supply Setup

To test the motors with a variable frequency pure sinusoidal waveform, a DC Motor coupled with a Synchronous Generator (Genset) was commissioned[2].

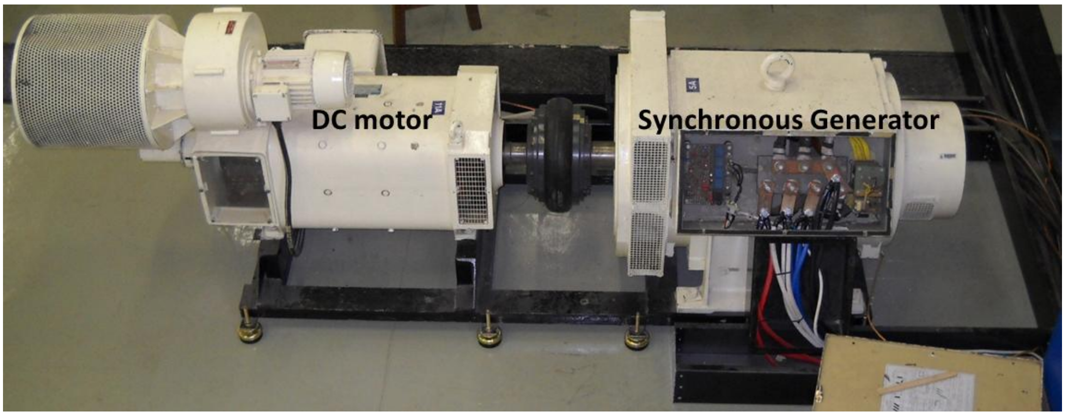

Figure 3.1: DC motor and Synchronous generator set (GENSET)

The DC motor within the Genset was setup together with a Variable Speed Drive, details can be found in Appendix A. This Genset within the laboratory was expected to provide balanced 3-phase waveforms. To make certain that these voltage waveforms were balanced, the percentage unbalance of Genset outputs (U_a, U_b, U_c)

---

[2] The reason that a variable transformer (Variac) could not be used is that the Variac would output a fixed frequency, and transformers with high enough power ratings were unavailable.

in the system (Figure 3.2) is evaluated according to the IEC/SABS standard [16]. The tests found that the supply was balanced with less than 0.05% unbalance. Details about this test can be found in section A.3.3 in Appendix A.

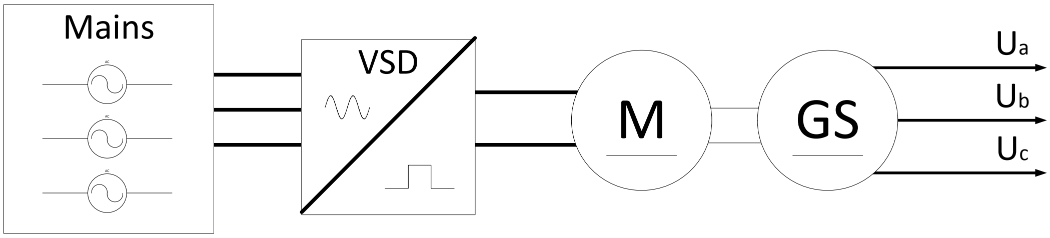

Figure 3.2: Genset circuit diagram

3.1.2 DSpace

The experimental setup makes use of dSpace, which is a real-time interface. DSpace allows for measurements to be viewed, stored and analysed on the desktop PC. It has further advantages such as the ability to rapidly prototype control systems for testing the motor, this will be important in future work when multiple control strategies will need to be implemented. A wide variety of measurements can be instantaneously taken by the dSpace system, which significantly speeds up the measurement process. The integration of dSpace into the complete system can be seen in Figure 3.3.

Other apparatus included:

- IM (stator and rotor)
- RSM rotor, both of which have been explained in the previous chapters
- A second synchronous generator, for loading the motors under test
- Resistor bank
- Torque sensor, unique to the setup which helped to validate the torque output and speed up further tests.
- Shaft encoder, which gave an accurate measurement for speed.

- Measurement equipment such as multi-meters, differential probes to confirm the measurements taken in dSpace.

It was important to analyse the accuracy of the measurement transducers, such as the torque transducers, shaft encoder, differential probes and current clamps. This analysis is shown in Appendix B.

3.2 Motor Test Setup

The Genset in the laboratory provided a variable amplitude/frequency pure sine wave as the input voltage to the IM. This was connected to the synchronous generator, via a torque sensor placed on the shaft. A shaft encoder was connected to the synchronous generator so that the speed of rotation could be accurately measured. The complete system setup is shown in Figure 3.3.

The speed and the torque measurements were used to calculate the total output mechanical power, which is useful in calculating the efficiency. These measurements and those of the voltage and current were connected to dSpace so that the data could be logged. This data was used to accurately test the motor's performance.

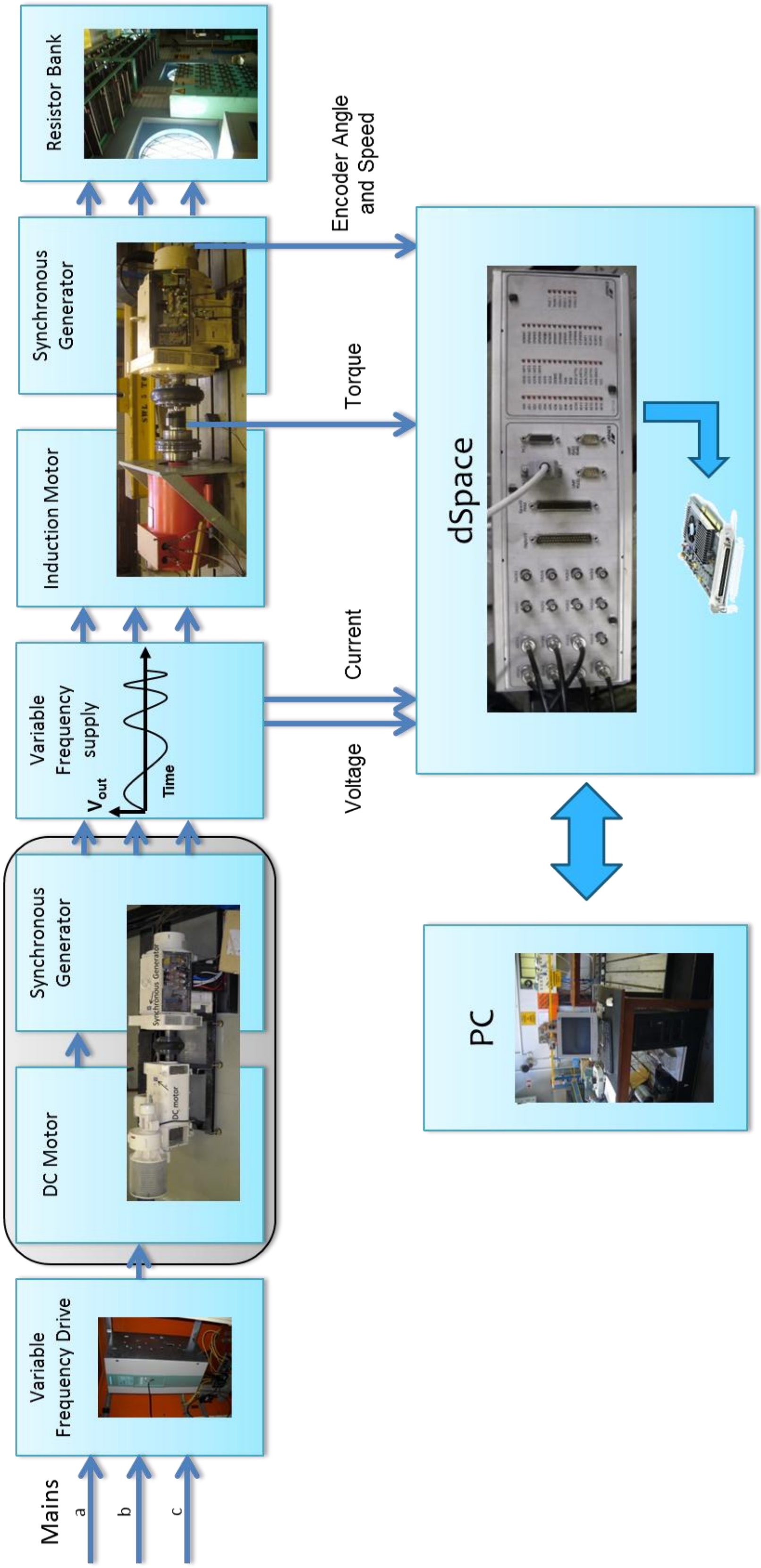

Figure 3.3: Complete System setup

3.3 INDUCTION MOTOR TESTS

The performance of the IM[3] was quantified using the well-known routine tests, like the:

- No load test.
- Locked rotor test
- Full load tests

Furthermore variable loads were also placed in order to get a more complete efficiency representation of the motor. This loading was achieved using another synchronous generator connected to a resistor bank, which is shown in Figure 3.4. These tests helped to populate the values in the equivalent circuit model for the system. The step by step application of these tests is provided so that the process of obtaining the losses is understood and is available for further comparative analysis of the two motors.

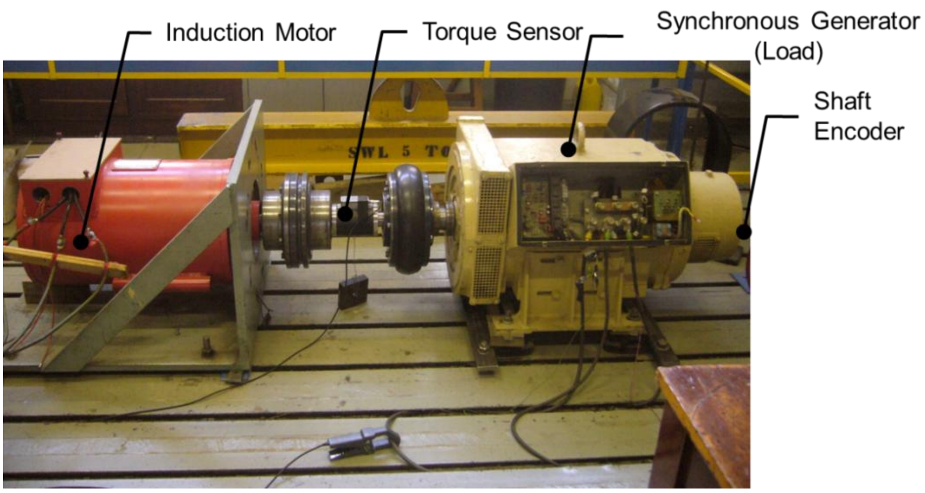

Figure 3.4: Laboratory test setup

[3] The IM was delta-wound, however a star/wye load formation was used to simplify the calculations (for per-phase quantities) as a neutral point was available on the Genset. To transfer to the delta equivalent circuit parameters, a $\sqrt{3}$ can be incorporated where appropriate.

3.3.1 IEEE Equivalent Circuit

The IEEE standard equivalent circuit (Figure 3.5) model parameters [17] are populated using the No-Load and the Locked Rotor tests. These standardised tests help to give the maximum and minimum performance characteristics of the motor.

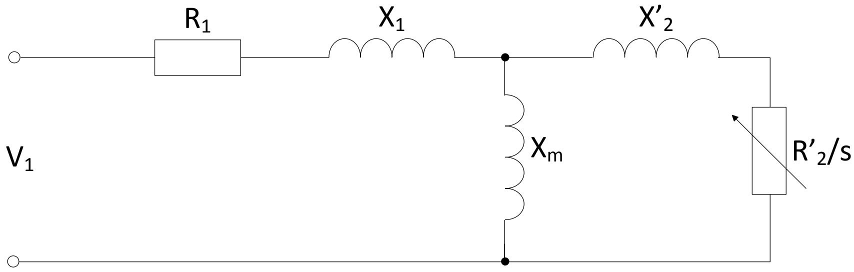

Figure 3.5: IEEE Equivalent circuit model for the IM

3.3.2 No-Load Test

During the No Load test, the motor is connected without a load. This allows for the types of losses associated with the motor construction to be quantified. These losses [17,18], include:

- Core Losses, this comprises of both hysteresis and eddy current losses.
- Friction, incorporating mechanical bearing friction.
- Windage Losses, based on air resistance losses

This test is done by allowing the motor to run freely, and monitoring the voltage, current and power. The measurements for the No-Load Test are:

Phase Voltage	251.6 V
Phase Current	33.03 A
3ϕ Input Power	3.546 kW
Line Resistance	0.13 Ω

The output mechanical power and the power loss through the windings (copper losses/I^2R losses) are subtracted from the input power, according to the equation 1.

$$P_{Rot} = P_{IN} - P_{OUT} - 3I_{phase}^2 R_{phase} \\ = 2670.86\ W \quad (1)$$

At the rated voltage, the rotational loses are 2.67 kW. These rotational losses are composed of mechanical losses (friction and windage) and electrical losses (core loss). These losses can be separated by reducing the voltage below the rated amount in regular steps and measuring the input power.

At the lower voltages the core losses become smaller. This is because the core loss is proportional to the square of the flux density, and the flux falls with the reduction in voltage [18]. By extrapolating the input power to the point at which voltage is zero, the core losses become zero and the remaining power losses is due to windage and friction.

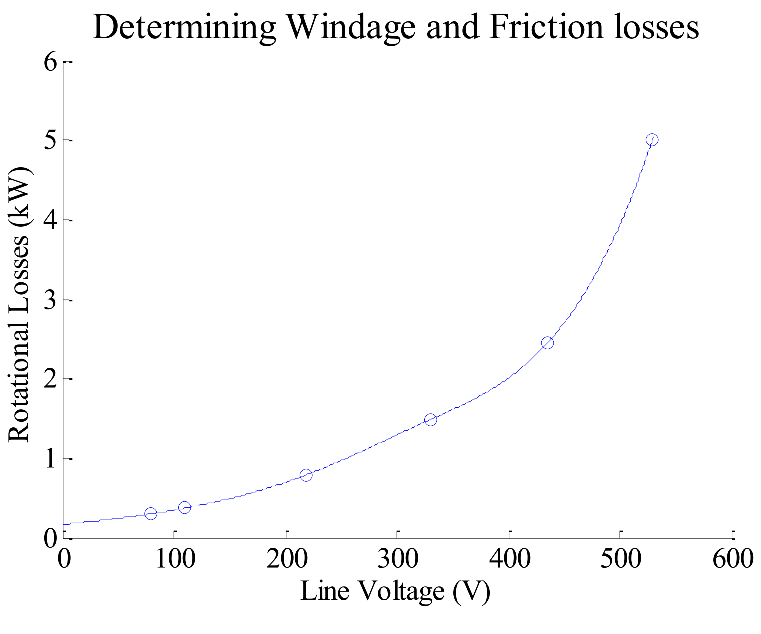

Figure 3.6: Splitting mechanical losses from electrical losses

The figure shows that the friction and windage losses account for 164 W. This means that the overall core loss at rated voltage is 2506.86 W (2670 kW – 164W).

Using the No Load test

Under the No Load condition, the series branch can be neglected as the R'_2/s is large [17] (because of a smaller slip) and information about the magnetisation branch is obtained. The parameters of the IEEE equivalent circuit that are obtained from the No Load test are shown in Figure 3.7.

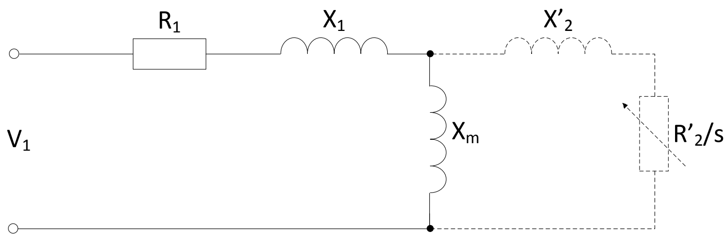

Figure 3.7: Parameters obtained from the No Load test.

The total No Load impedance is

$$Z_{NoLoad} = \frac{V_P}{I_P} = 7.62\ \Omega \tag{2}$$

The No Load resistance is

$$R_{NoLoad} = \frac{P_{NL}}{3I_P^2} = 1.08\ \Omega \tag{3}$$

The No Load reactance is therefore calculated using Equations 3 and 4.

$$\begin{aligned} X_{NoLoad} &= (Z_{NoLoad}^2 - R_{NoLoad}^2)^{1/2} \\ &= 7.54\ \Omega \end{aligned} \tag{4}$$

The fact that $X_{No\ Load}$ is equal to X_1+X_m, is later used to split the reactance [17].

3.3.3 Locked rotor test

The locked rotor test, tests the motor by placing the maximum amount of load on the motor. This test gives us information such as leakage impedances of the motor. The test is done by locking the rotor in place by using a metal rod. This test needed to be done quickly as the motor could "burn out". The measurements for this test are:

Phase Voltage	43.35 V
Phase Current	94.35 A
3ϕ Input Power	4.709 kW
Torque	13.67 N.m

The per phase starting current (559.9 A) is obtained by extrapolating the line current to the point of rated voltage[4].

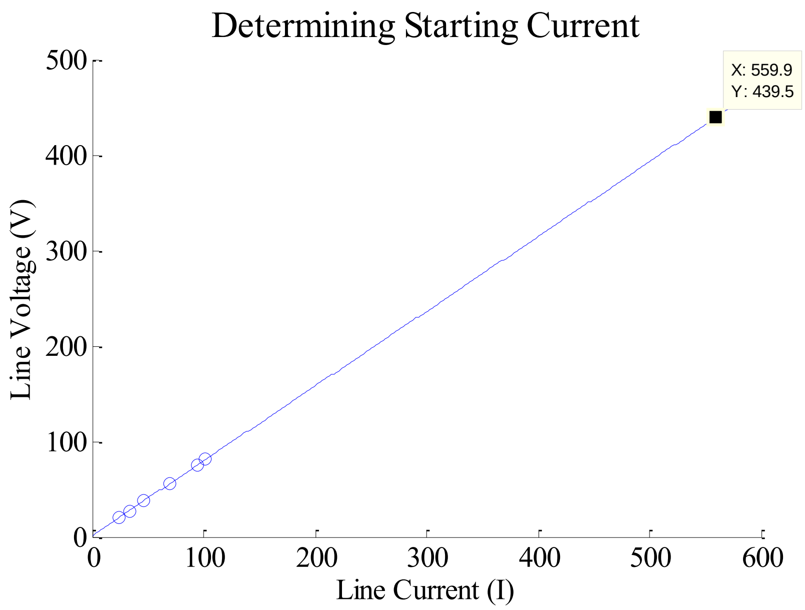

Figure 3.8: Determining the per phase starting current

The starting torque can also be calculated by proportioning the torque by the voltage squared [19].

$$\begin{aligned} \tau_{start} &= \frac{\tau_{LockedRotor} V_{start}^2}{V_{LockedRotor}^2} \\ &= 469.39\ N \cdot m \end{aligned} \tag{5}$$

This starting torque (469 N.m) calculation is substantially higher than those predicted in the simulations (355 N.m) [10]. The disparity is explained through the concept that FEM analysis in [10] incorporates the saturation effects within the

[4] This would need to be changed when transferring to the delta-wound circuit values.

material while the extrapolation assumes linear square relationship, without taking saturation effects into account. Therefore the FEM results from the design (355 N.m), which take the saturation effects into account, are taken as the torque benchmark for the IM.

Using the Locked Rotor Test

The parameters of the IEEE equivalent circuit that are obtained from the Locked Rotor test are shown in [17].

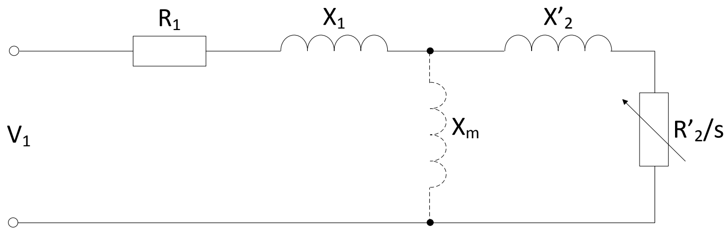

Figure 3.9: Parameters obtained from the Locked Rotor test

The total Locked Rotor Impedance is determined in Equation 6, similar to the way in which the No Load Impedance was calculated above.

$$Z_{LockedRotor} = \frac{V_p}{I_p} = 0.46\ \Omega \tag{6}$$

The Locked Rotor resistance is determined in Equation 7, using the power and current quantities.

$$R_{LockedRotor} = \frac{P_{LockedRotor}}{3I_{Phase}^2} = 0.18\ \Omega \tag{7}$$

The Locked Rotor reactance is also calculated in a similar manner.

$$\begin{aligned} X_{LockedRotor} &= (Z_{NL}^2 - R_{NL}^2)^{1/2} \\ &= 0.42\ \Omega \end{aligned} \tag{8}$$

This reactance can be further split up to determine the magnetisation impedance.

$$X_{LockedRotor} \simeq X_1 + X_2'$$

$$X_1 = X_2' = 0.21 \qquad (9)$$

$$X_m = X_{NoLoad} - X_1$$
$$= 7.33$$

Using the magnetisation impedance, R_2 can also be determined.

$$R_2' = \left(\frac{X_2' + X_m}{X_m}\right)^2 (R_{BL} - R_1) \qquad (10)$$
$$= 0.12\,\Omega$$

3.3.4 Full-load Test

The purpose of the full load tests is to determine the efficiency of the motor. This helps to determine the losses at each stage of the power transformation process, from electrical to mechanical, Figure 3.10.

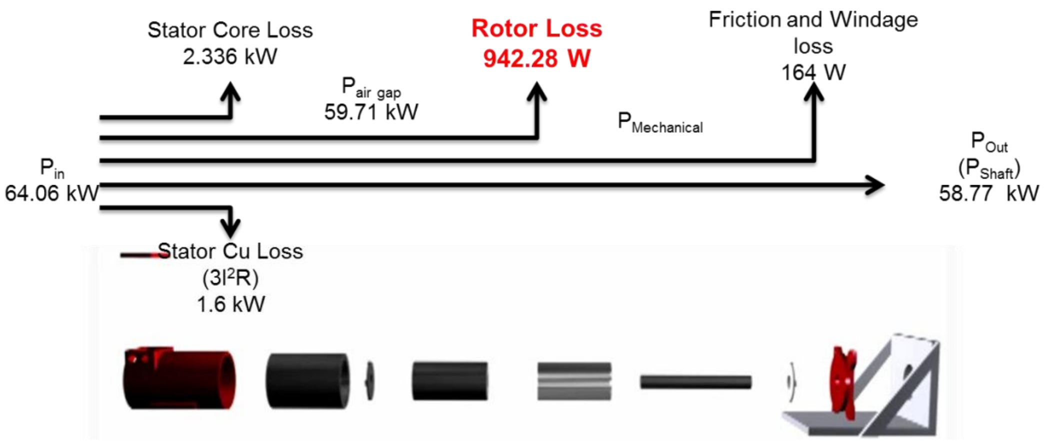

Figure 3.10: Losses and efficiencies at different stages of the induction motor. (The rotor loss is expected to be reduced when using an RSM rotor)

One of the ways of doing this is by calculating all the losses in the motor, and then subtracting these losses from the input power.

The Copper/Winding losses are calculated as shown

$$P_{Cu} = 3I_P^2R \qquad (11)$$
$$= 1686.56\,W$$

These losses are then used, together with the rotational losses calculated from the No Load test, to determine the overall power across the air gap.

$$P_{Airgap} = P_{IN} - P_{Rot} - P_{Cu}$$
$$= 59.71\ kW \tag{12}$$

The Slip is the difference in speed between the synchronous speed (the speed of an ideal motor) and the actual speed of the motor.

$$s = \frac{n_s - n}{n_s}$$
$$= 0.0155 \tag{13}$$

The Slip is used to determine the losses within the Rotor.

$$P_{Rotor} = P_{Airgap} \times \frac{s}{1-s}$$
$$= 942.28 \tag{14}$$

The output power is then determined by subtracting all the losses from the input.

$$P_{out} = P_{in} - P_{Rotor} - P_{Cu} - P_{Rot}$$
$$= 58.77\ kW \tag{15}$$

Finally the efficiency is determined as the ratio between the output power by the input power.

$$\eta = \frac{P_{out}}{P_{in}}$$
$$= 91.74\% \tag{16}$$

Another way to determine efficiency was by using the torque measurements (from the torque sensor) and the speed measurements (from the shaft encoder). Mechanical Power is equal to the Torque multiplied by the Angular Velocity, as shown in the equation below [17].

$$P_M = E_a I_a = T\omega_m \tag{17}$$

The efficiency calculated using the mechanical output power using the torque sensor is shown below.

$$\eta_2 = \frac{P_{Out\ Mechanical}}{P_{in}} = 91.31\% \tag{18}$$

The two values for efficiency correspond. One was determined using the subtraction of losses (19) and the other using the mechanical output (21). The small difference can be accounted for by considering stray load losses. These losses were not incorporated in to the subtraction of losses method. According to standards [20], stray load losses are approximated to be 0.5%. These losses explain the difference (0.43%) in the values for efficiency.

Further tests for efficiency, based on well documented standards [19], were done using the torque sensor (mechanical output) at lower input power levels. This was done by loading the motor with a synchronous generator, and choosing four equally spaced load points between 25% and 100% rated load [19]. These points were selected to be at approximately 25%, 50%, 75% and 100% of rated electrical input power, and observing the output mechanical power.

The results (Figure 3.11) showed that even at lower power levels, the motor was highly efficient. This means that the induction motor is a tough motor to improve upon and demonstrates why it has dominated the motor market.

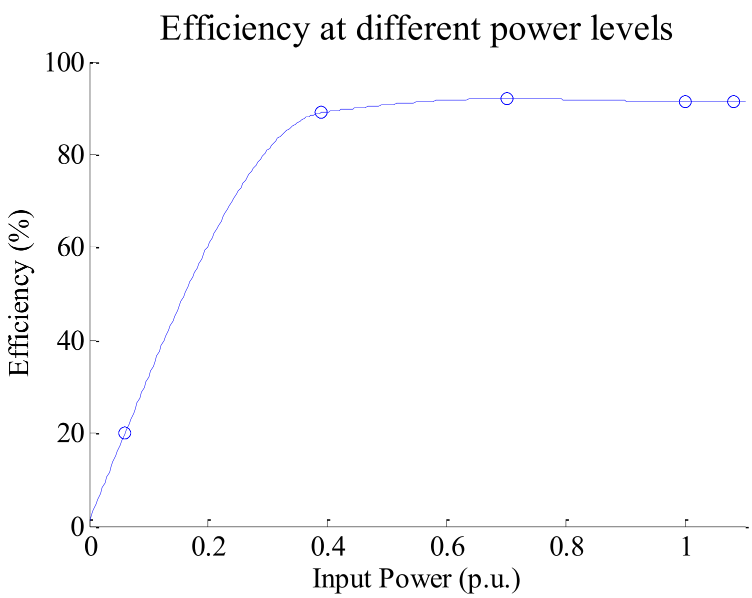

Figure 3.11: Efficiency at lower power levels

3.4 Analysis of Induction Motor Tests

The results show that this sample Induction Motor is a highly efficient motor (92%). However, at a rating of 55 kW even a small loss of 8% equates to an overall loss of 6 kW. This overall loss is expected to be reduced by using a RSM.

3.5 RSM test setup

The RSM cannot be directly powered from the variable frequency 3 phase supply system. This is because the RSM requires the resultant flux vector to operate at a precise angle that creates the maximum torque. To achieve this, an intelligent supply/control system (implemented using a VSD) is required. This supply would determine which coils should be energised (based on the rotor position/saliency) so that the correct resultant flux vector is maintained.

In order to develop this intelligent supply system, static inductance and torque measurements for the RSM were taken. These measurements were done by replicating a snapshot in time of a 3-phase condition (Figure 3.12a and b). This was done by connecting two terminals of a 3-phase motor in a way that ensures that the current flow through the terminals represents the 3-phase condition. The condition being simulated ensures that peak current passes through one phase and half of the peak current flows through the other two phases in the reverse direction.

This physical two terminal connection enforces this 3-phase condition, in the delta winding. This was the condition under which the measurements were taken.

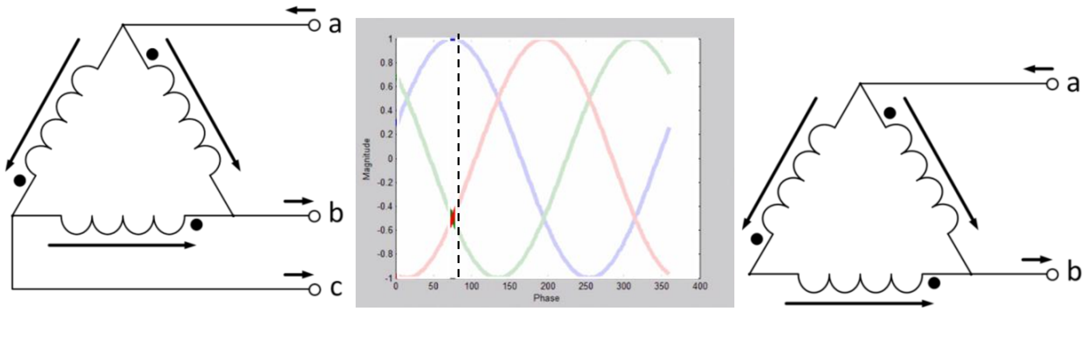

a. b. c.

Figure 3.12: a) 3-phase terminal connections, b) at a snapshot in time of 3-phase condition being replicated by a c) two terminal connection.

3.6 Reluctance Synchronous Motor Tests

For the RSM, measurements for the inductance and torque are taken.

3.6.1 Inductance Measurements

The rotor has a specific pattern which gives the rotor saliency, Figure 2.4. The actual profile of the rotor has areas that are highly reluctant (low inductance due to air gaps) and areas which have a low reluctance (high inductance due to steel). This means that knowledge about the rotor position can be determined by measuring the inductance (using an LCR meter[5]) between the two terminals.

[5] The current excitation is not considered to be large enough to setup a significant magnetic field.

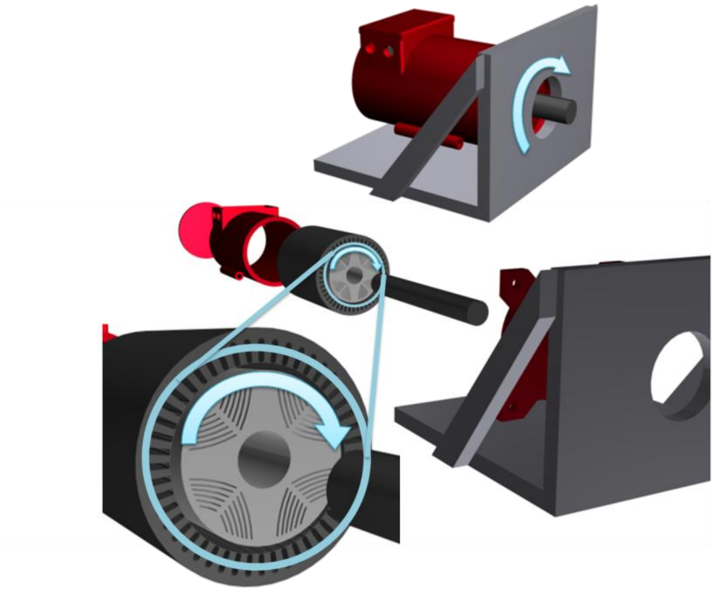

Figure 3.13: Process of taking measurement for the RSM.

The inductance is initially measured across two terminals, by rotating the rotor by 10 degrees and measuring the inductance (Figure 3.13). By observing these measurements, a pattern emerges which corresponds to the air-gap pattern on the rotor. The graph in Figure 3.14 shows the measured inductance with the rotor at different positions. The graph clearly shows that the inductance pattern repeats after every 90 degrees, which corresponds to the cut-out pattern in Figure 2.4.

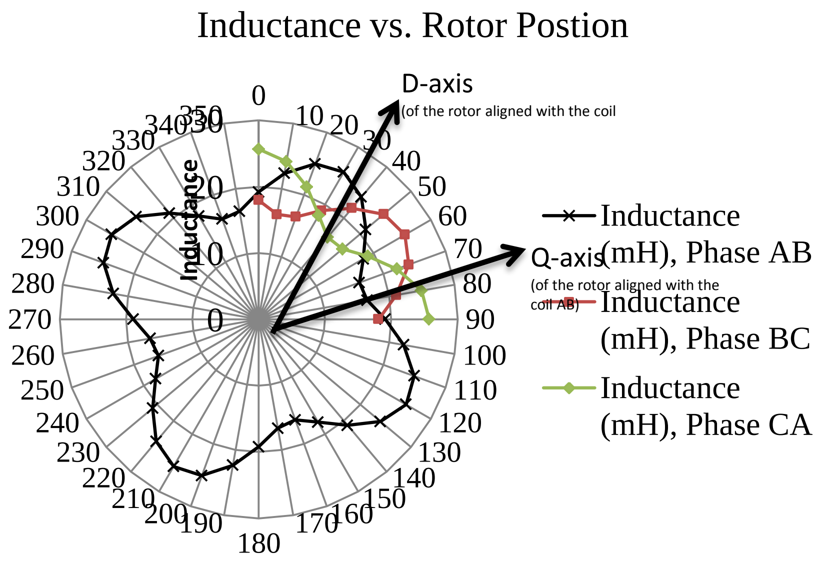

Figure 3.14: Inductance measurements across terminals.

This helps determining where the least reluctance and maximum reluctance regions are within the rotor. This inductance information also helps in being able to limit the measurements to the first 90 ° as the pattern would repeat. The inductance for the different phases is also measured, for the first 90 degrees to confirm the difference in the each coil's location.

The inductance is shown on a polar plot to show the inductance as a function of the angle. The peak inductances are measured when the winding aligns with the least reluctant area (metal) on the rotor and the lowest inductance occur when the winding is aligned with highest reluctance (air-gaps).

Further analysis of these measurements is provided in the next chapter.

3.6.2 Torque Measurements

The torque is measured by applying a DC current through the two terminals, which ensures that the snapshot in time of the 3-phase condition is maintained. The torque is then measured using the torque sensor with the rotor being locked at successive rotor positions (10 degree increments, similar to the inductance measurements). As the torque is locked in different physical positions it ensures that the measurement axis (stator coil) aligns with every point on the rotor, which provides information about where the maximum torque lies.

The inductance graph (Figure 3.14) showed that a single D-q sector lies between 30 and 75 degrees in terms of the physical rotor position, and that it repeats every 90° (because of the rotor pattern). Therefore, the torque produced in this one sector was studied, as the other sectors should replicate these results. The graph in Figure 3.15 shows that the torque produced is dependent on the rotor position as the rotor has saliency.

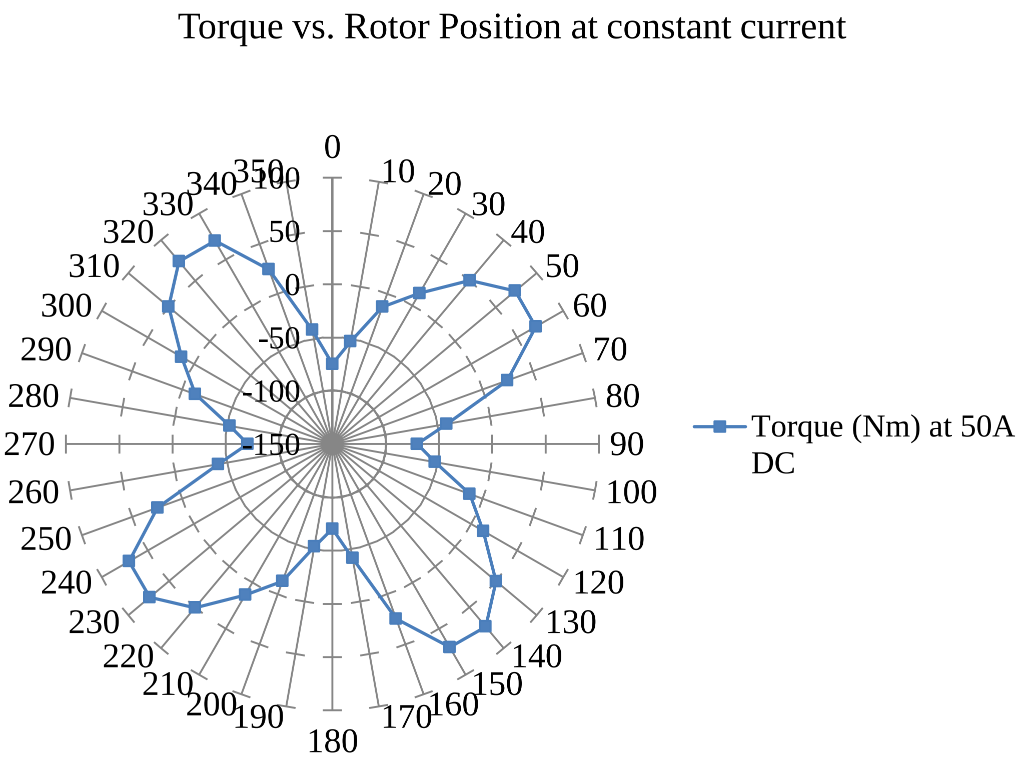

Figure 3.15: Measured torque at different angles.

D-q axes shown in the figures represent the physical rotor axes aligning with the measurement coils (in this case coil AB). The difference between the d and q axis, in the rotor (physical) reference frame is 45°, as opposed to the 90 electrical degrees. The results obtained through simulation stated that the maximum torque angle should occur at about 60 electrical degrees. Therefore, the 60 electrical degrees would (by coincidence) correspond to 60 physical degrees (30+60/2=60).

This information can be used to develop an intelligent power supply, which ensures that the resultant vector is maintained 30° ahead of the point of minimum reluctance (60° in the electrical d-q reference frame). This would ensure that maximum torque is generated by the motor, so that the performance can be accurately compared with the induction motor.

The graph in Figure 3.16 shows the torque and inductance graphs on a common position axis. The first 90° of measurements (Figure 3.16) indicate that a higher torque is generated, at the points where the inductance vs. position graph has the maximum gradient. This confirms the theory that the maximum torque is generated when the rate of change of inductance results in the highest torque.

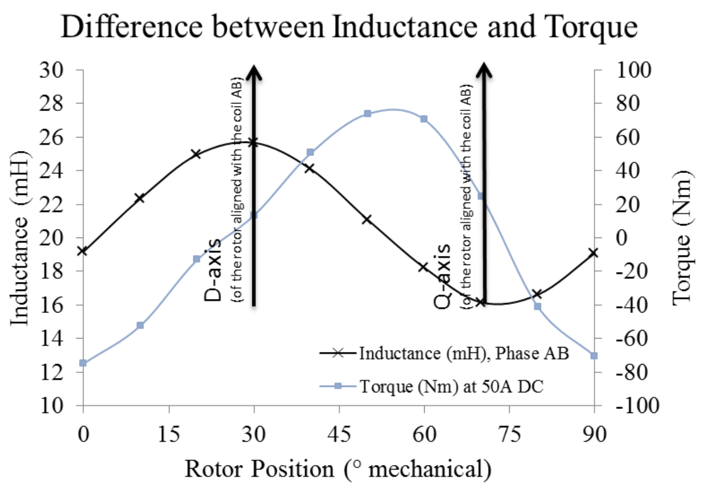

Figure 3.16: Inductance and Torque measurements, over the first quarter revolution of the rotor. D-Q axis represents the area in Figure 2.4.

A range of measurements were done by varying two parameters, the input current, rotor position and observing the resultant torque. The torque was measured at every 10 degrees from 0 to 90, and is shown in Figure 3.17.

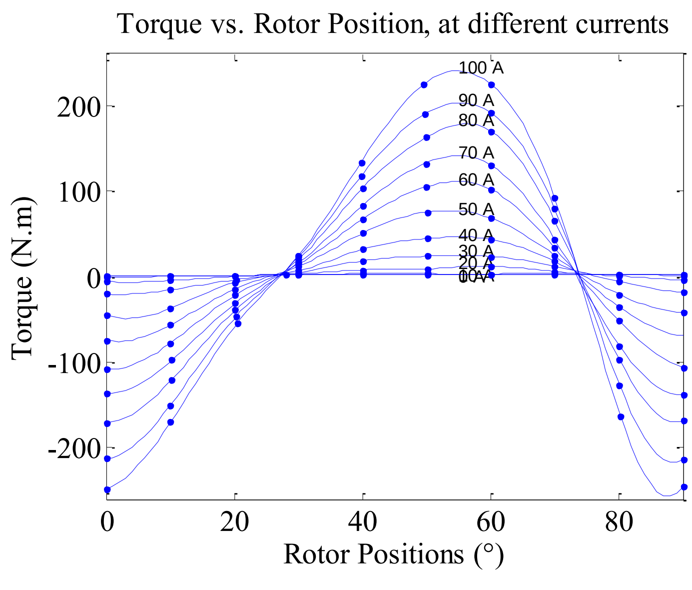

Figure 3.17: Torque produced in different rotor positions (mechanical degrees).

These measurements show that the results are mirrored across 45 degrees which corresponds with the reflection on the rotor construction Figure 3.18.

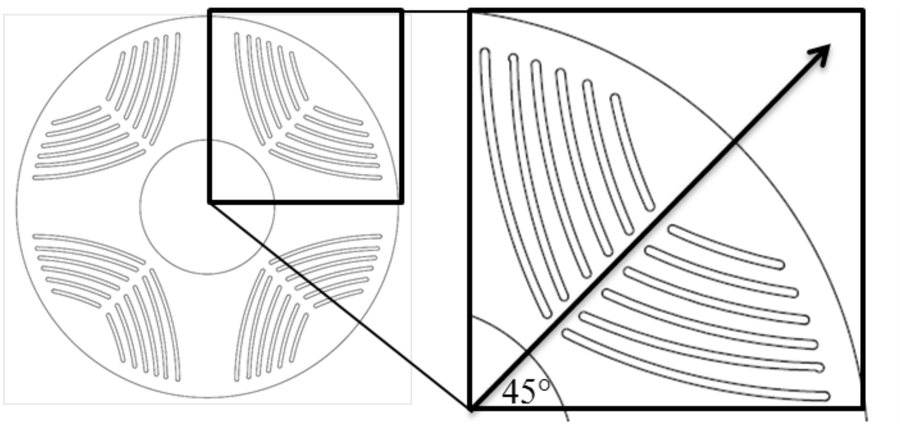

Figure 3.18: Reflection of the air gap cut out pattern on the rotor.

A zoomed in view of these angles (in mechanical degrees) is shown in Figure 3.19.

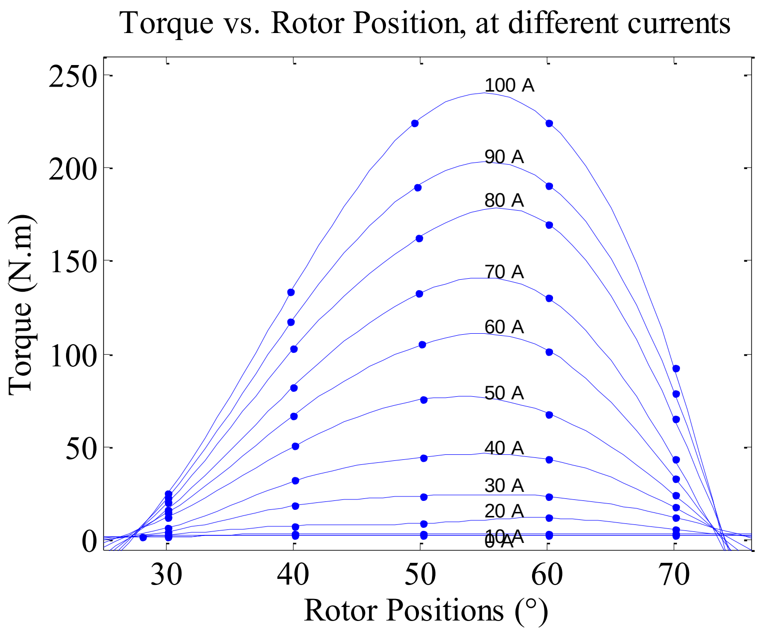

Figure 3.19: Torque produced in different rotor positions, between 30 and 75 mechanical degrees

These results validate the initial design that was done. The initial design's simulation results [10] obtained through Finite Element Analysis are shown in Figure 3.20 (with respect to electrical degrees).

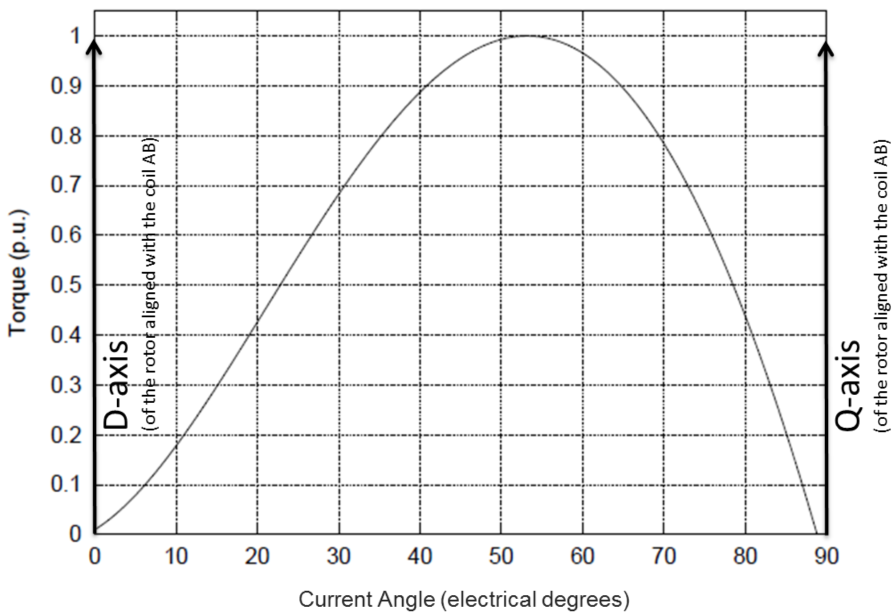

Figure 3.20: The simulated torque curve [10] in electrical degrees, D-Q axis as in Figure 2.4.

The results from this single D-q sector show that the angle at which the maximum torque is generated is close to 60^o (physical degrees). To determine this angle more precisely, further measurements were taken in order to determine where the maximum torque is generated. These additional measurements were taken from 55 to 65 degrees, and are shown in Figure 3.21.

These extra measurements show that the maximum torque angle is at 56^o (physical degrees). The simulation predicted that the maximum torque angle should lie at 53 electrical degrees. In order to convert this into physical degrees, the maximum torque is expected to 30+53/2=30+26.5=56.5^o on the physical rotor. Thus, the quantities predicted through simulation, match the measured values again.

The torque vs. position profile matches well with the simulation predictions. As the angles at which maximum torque will occur, correspond with those predicted in simulation. However the profile does appear to have some jaggedness and is discussed in greater detail in the next section.

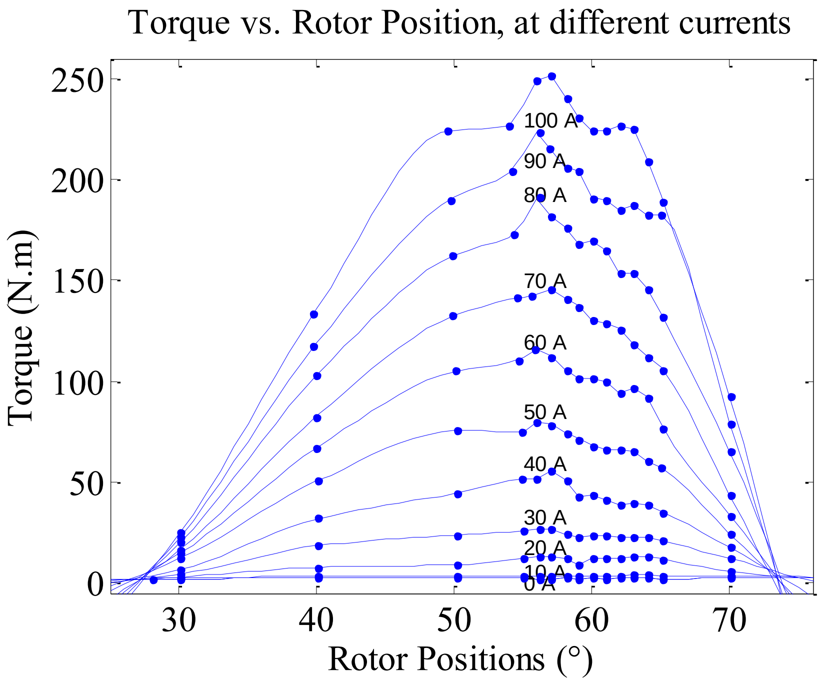

Figure 3.21: Torque produced in different rotor positions, between 50 and 75 mechanical degrees

The magnitude of the torque appeared to be substantially lower than normal, this is because DC currents that were equivalent to the RMS values of the sin waves, were used for the measurements. However the RMS values are not representative of the three phase snap shot in time of the sine wave that is supposed to be simulated by the DC currents. This would only be achieved if the DC current was equivalent to the peak current, Figure 3.12. Figure 3.22 below, demonstrates this effect in greater detail.

This finding requires further tests to be done at DC currents which represent the peak voltages as opposed to the RMS voltages. For these measurements the inductance was also measure in one degree increments in order to be able to convert between electrical and physical degrees more precisely.

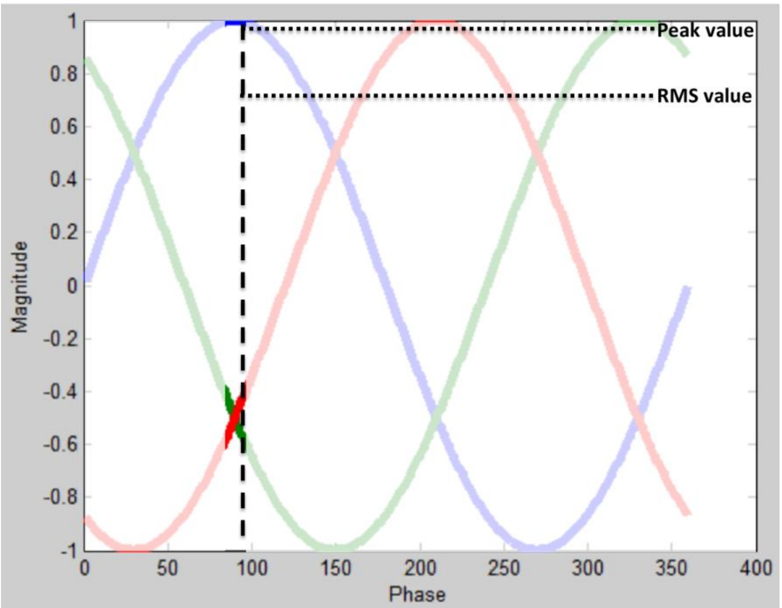

Figure 3.22: Difference between DC currents that are equivalent to RMS or peak currents.

3.6.3 Further measurements

The inductance was again measured, this time in one degree increments to gain greater insight into the saliency ratio ξ (ratio between maximum and minimum inductance). Equation (22) describes the saliency ratio [21].

$$\xi = \frac{L_d}{L_q} = \frac{24.43}{15.157} = 1.612 \tag{19}$$

The measurements for the inductances are shown in Figure 3.23, and show smooth inductance results corresponding to the rotor cut-outs.

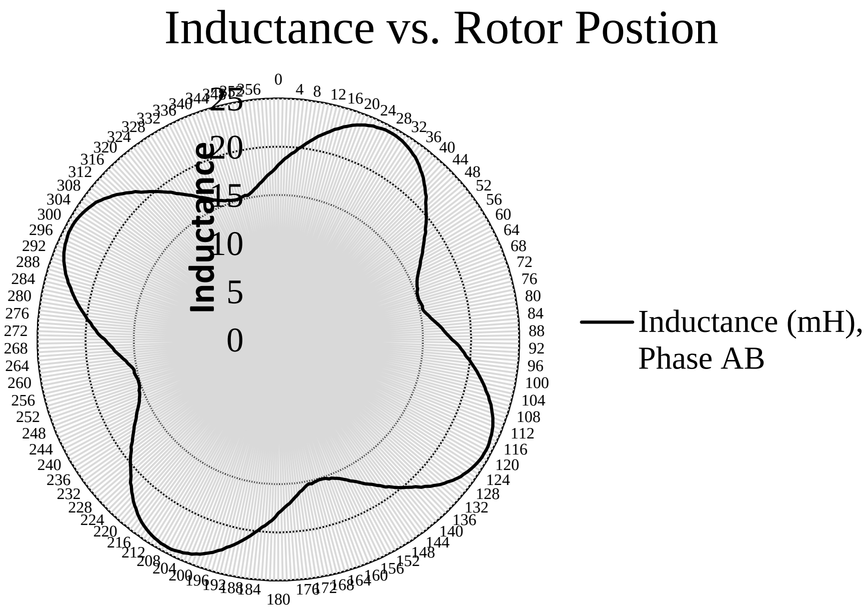

Figure 3.23: Inductance Measurements at every degree of physical rotation.

The torque measurements (also in one degree increments) for higher current levels are shown in Figure 3.24. The one degree increments were to quantify the torque at rated current more accurately as well as find out whether the jaggedness of the torque measurements found in Figure 3.21, repeats at other angles.

These measurements were done under DC currents that were equivalent to the peak current (that occur at rated RMS current). In the figure, the RMS values are stated so that an appropriate comparison can be drawn with the induction motor, while the peak currents represent the actual DC current that was supplied to get the measurements. These same torque measurements are also shown on a 3D plot, Figure 3.25, so that the variables can be seen more clearly.

The graphs show that the RSM can produce 368.5 N.m of torque at the equivalent rated current 93 A of the IM. And at 129% of rated current the RSM can produce

510 N.m of torque. These results are discussed in more detail in Section 4.1.2: Torque Production.

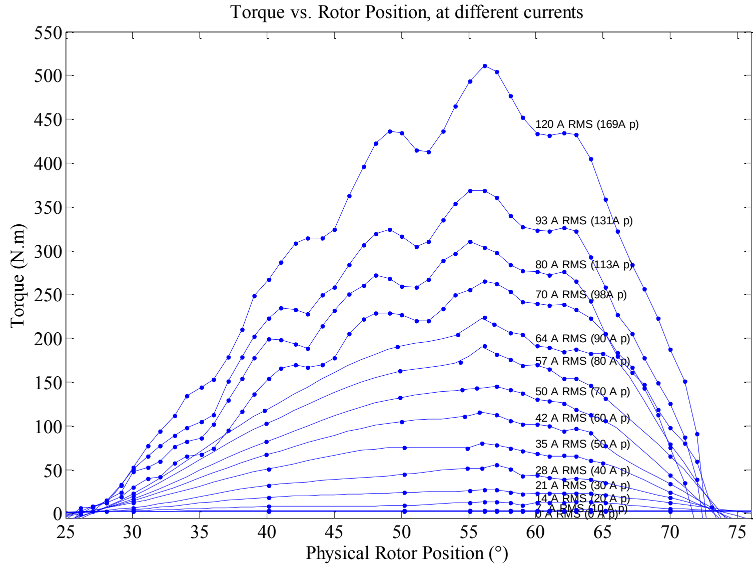

Figure 3.24: The torque measurement under DC currents in mechanical degrees (with labels for equivalent peak and RMS currents for comparison purposes).

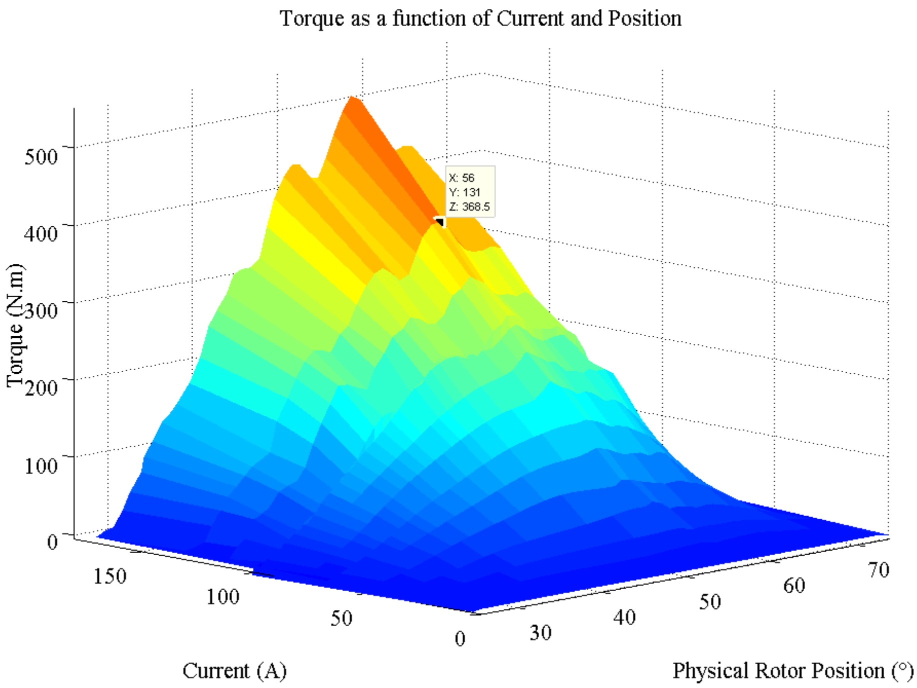

Figure 3.25: 3D plot of the torque measurement under DC currents and different rotor positions (mechanical degrees).

3.7 Summary

This chapter details the setup, the experiments and the results from those experiments. Analysis of these results is presented in the next chapter.

Chapter 4

Analysis

The last chapters discussed the motors in terms of their construction and the experiments that were performed. This chapter collates and analyses the evaluation of the two motors.

4.1 Motor Evaluation

The induction motor is a highly efficient motor which is tough to improve upon. While improving upon the IM itself is difficult, large improvements can be made when looking at the complete and overall system. The complete system integration of the VSD and the IM was analysed for a specific mine-shuttle application (considering the VSD is important when evaluating RSMs as an alternative solution, as the RSM requires a VSD[6] to operate).

The table below collates and highlights the advantages that the RSM has for the mine shuttle vehicle application.

Motor Characteristic	Induction Motor	Reluctance Synchronous Motor
Construction Cost	Good	Better[6]
Reduced Construction Complexity	Good	Better
Robustness	Good	Better
Torque Production	Good	Better
Efficiency	Good	Still to be quantified

[6] If the machines are individually compared, then the additional cost of the VSD with the RSM negatively affects the RSM.

More details about each of the characteristics analysed, will be covered in the following sections.

4.1.1 Construction

In terms of construction costs, the RSM requires less components in order to be manufactured, this was shown in Section 2.1 and Section 2.2.

When considering complexity of construction and the number of steps taken to actually produce the motor, the RSM also has reduced number of steps to actually manufacture the motor.

Furthermore in terms of robustness, the RSM also dominates this characteristic due to the reduced welding and construction steps. The reduction in the number of production steps also makes the RSM less susceptible to failure.

4.1.2 Torque Production

The results show that the RSM (368 Nm) can generate greater torque than the IM (355 Nm) [10] under the same current levels (93 A RMS). This is shown in Figure 4.1, which has been modified from Figure 3.24 to show the torque values in relation to electrical degrees.

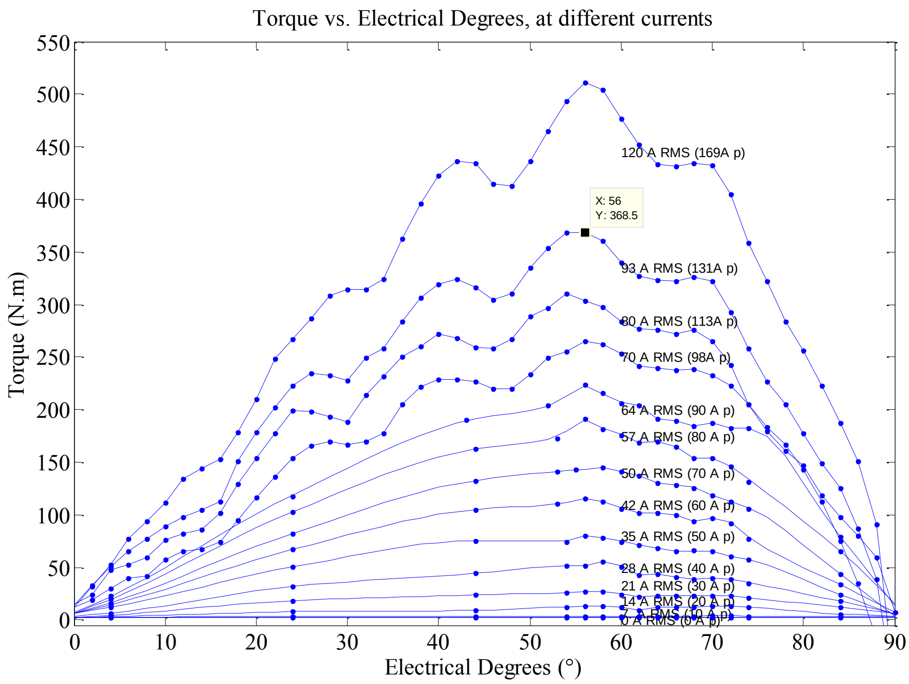

Figure 4.1: Torque measurements, converted to electrical degrees

This increase in torque means that an equivalent torque to the IM can be generated by the RSM at even lower currents. An additional advantage of the RSM is that the motor has reduced heat losses [15] (this means it does not heat up as much as the IM). Since the current rating of the motor winding is dependent on the winding temperature [22], it means that the RSM can handle larger currents [15]. Due to this, further torque measurements at higher current levels were also taken for the RSM. These measurements were taken at the equivalent of 120 A RMS (129 % of rated current) to determine the torque that is produced by the motor at higher current levels. At 129 % of rated current the RSM produces 510 N.m or 143.66 % larger torque.

Essentially the prototype RSM has a higher torque density than the IM, which means it can produce greater torque within the same motor frame (construction). Or a smaller RSM can produce the equivalent torque of an IM.

This capability of larger torque is slightly higher than the predictions of the initial design simulations. It was estimated in the design [10] that 42 % more torque could be generated at 140 % of rated current, while the results show that 43 % more torque can be produced with 129 % more current. This small difference in the results shows the effectiveness of FEM for rapidly prototyping new designs. This 11 % enhancement over the simulations can be attributed to:

- Construction material, the material used for construction is not the same as the material properties that were defined in the simulations. This could stop the motor from operating in saturation.
- Construction process, the initial simulations were based on the same lamination slices as those used for the induction motor. However the assembled rotor incorporates much thicker slices/slabs.
- The air-gap of the motor is lower than in the FEM design which could result in slightly higher torque.

A point to note is the jaggedness of the profile in the torque measurements. Under closer inspection, it is observed that, the difference between the peaks and the troughs of the jagged profile are eight physical degrees (16 electrical) apart. This corresponds with the actual physical rotor construction, and the stator slot sizing. The stator slot is shown in Figure 4.2.

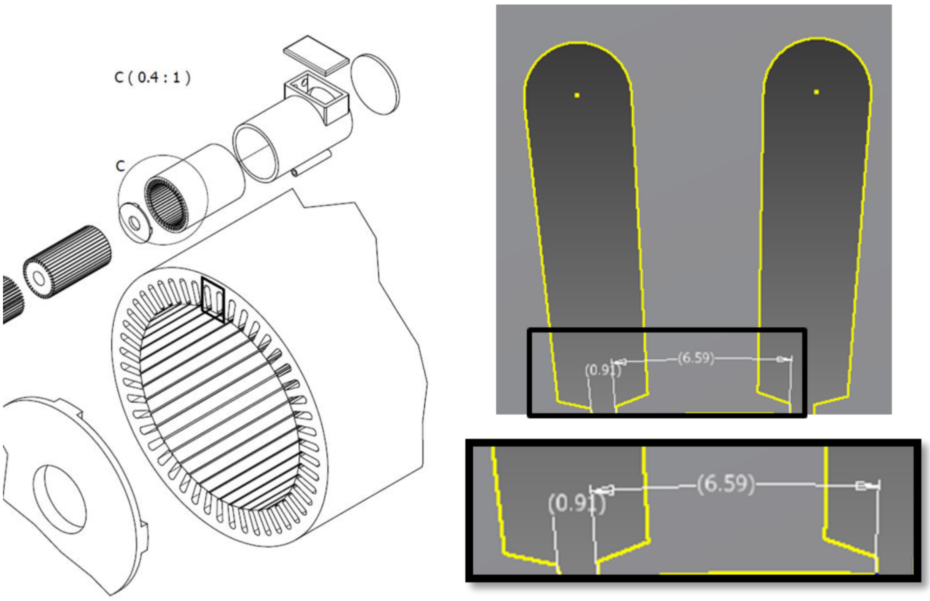

Figure 4.2: Stator slot width, in physical degrees

4.1.3 Efficiency

The efficiency of the motor still needs to be quantified as the motor requires a VSD with the correct vector control so that the motor can be operated at the correct torque angle. From the initial torque results it appears that the RSM will be more efficient.

4.2 Control

A number of control techniques are available for use in overcoming obstacles that could be in the way of a mine shuttle vehicle in underground mines, such as small rocks. One of these is using maximum torque control (MTC) [23], which would allow the RSM to generate the maximum torque. A maximum rate of change of torque (MRCTC) could also be designed for mine shuttle start-up and this could then switch over to a maximum power factor control (MPFC) which would increase energy efficiency. Further work could also be done into sensor-less control as the presence of an encoder increases costs as well as risks of the control system failing due to encoder failure [24].

4.2.1 Maximum Torque Control (MTC)

Maximum torque control ensures that the torque angle is positioned at a point where maximum torque will be generated. From the results for the RSM, this would be at 56^o electrical degrees which confirms the predictions made in the design [10].

4.2.2 Maximum Rate of Change of Torque Control (MRCTC)

The MRCTC angle as defined in [8,21,23] is shown in Equation 22.

$$\theta_i = \tan^{-1} \xi = \tan^{-1}\left(\frac{24.43}{15.157}\right) \tag{20}$$

This results in the angle being 59.7436^o. This is quite close to the MTC angle of 56^o. Analysing the graph, there is a higher gradient closer to 90^o, and this would have a much larger rate of change of torque. However the amount of torque generated close to this point is quite low, therefore having a large rate of change of torque closer to maximum torque is quite applicable.

4.2.3 Maximum Power Factor Control (MPFC)

MPFC is defined in [8,21,23] as shown in

$$\theta_i = \tan^{-1} \sqrt{\xi} = \tan^{-1}\sqrt{\left(\frac{24.43}{15.157}\right)} \tag{21}$$

This angle is at 51.7735^o. This is again close to the MTC angle.

4.2.4 Maximum Efficiency Control (MEC)

The MEC is defined [8,21,23] to be at 45^o.

The angles of these proposed control systems are shown on the torque graph in Figure 4.3. The graph shows that there is a large amount of flexibility, when considering the different types of control techniques. And that substantial torque can still be generated when operating at maximum efficiency or trying to control the power factor.

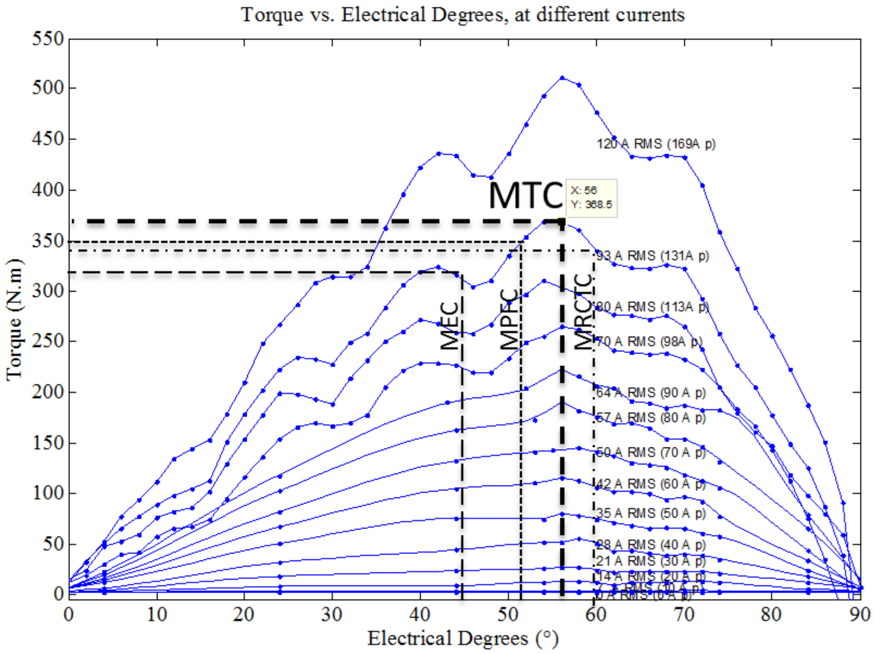

Figure 4.3: Application of different control techniques on the torque graph

4.2.5 Sensor-less Control

The defined saliency of the RSM as shown in Figure 3.23 shows the suitability of the RSM for sensor-less control as the rotor's position can be determined by the inductance as opposed to having an external shaft encoder. This would further increase the robustness of the RSM motor system, which would be advantageous in a mining environment.

4.3 Mine Shuttle Application

When the above analysis is compared in terms of the actual application the RSM compares very favourably. As torque is the primary factor of concern in a mine shuttle (1.3.1 Generating thrust), the RSM shows its dominance in this regard, by being able to produce the 13 N.m more torque than the IM as well as having a more robust construction. By having lower construction costs and complexity the RSM also improves its advantages over the IM in this regard.

4.4 Implications of the research

This work can lead to many positive social effects, particularly in the energy sector. The torque production and construction advantages of the RSM were highlighted and show the motor to be both cost effective as well as energy efficient. This research can have a very direct result on the local South African economy if further RSM research is conducted by the local mine shuttle motor manufacturer. This would also help to further develop the local manufacturing industry and thus providing more jobs.

These advantages of the RSM are not only limited to mine shuttles but also be very useful in other industries and industrial applications which already use the IM and VSD combination. If large enough numbers of IMs are converted to RSMs it may result in a significant reduction in industrial energy demand globally. This reduction in South Africa could result in less electricity demand required from power stations. This would not only result in less pollution (as the majority of power stations in South Africa, run on coal), but may also save the South African tax payer significant amounts of money as fewer power stations would need to be built in the future.

By implementing energy saving motors it is estimated that enough energy could be saved to power 1500 average households [4]. Furthermore, an energy cost is also associated with manufacturing the motor. By reducing the materials required in manufacturing the IM and the number of assembly operations, the overall energy footprint of the motor can be reduced.

The mine shuttle vehicle case study is also useful for the future of electric vehicles. Electric vehicles are commonly seen as the next generation of the transport industry. This research has shown that the RSM would provide a high output torque while providing a cost effective solution for electric vehicles which already use VSDs. This would not only make the newer vehicles efficient and more environmentally friendly but would also make the vehicles more financially accessible. Thus, previously marginalised sectors of society would be empowered by having readily available (public or private) transport to develop industries. This price advantage would also help the countries in Africa to increase industrialisation.

4.4.1 Axial Flux Reluctance Synchronous Machine

An interesting development from the work (for electric vehicles) is the idea of an axial flux reluctance synchronous machine, with a simplified construction process. One of the key advantages of the RSM that the research highlighted was the reduced construction cost while offering greater torque. This reduction of cost was primarily because of the optimised rotor design and construction. Based on this rotor design and using an ad-hoc analysis of the radial flux rotor, an improved construction of an axial flux rotor is proposed. The following represents the radial flux machine and its axial flux equivalent with the reluctance paths.

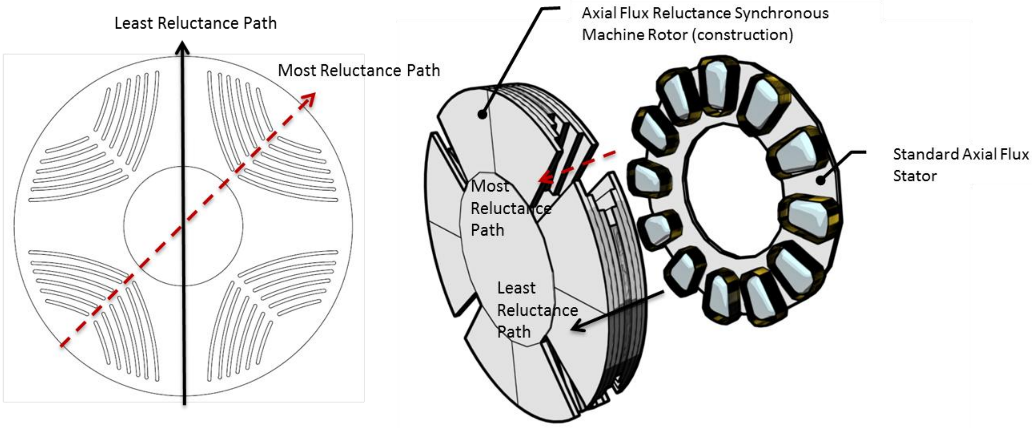

Figure 4.4: Reluctance paths in the radial RSM and its axial flux equivalent.

The axial flux RSM can be manufactured with a number of laminations that could be cut out in a specific pattern, and stacked together, to create paths of varying reluctance. This construction method is shown in Figure 4.5.

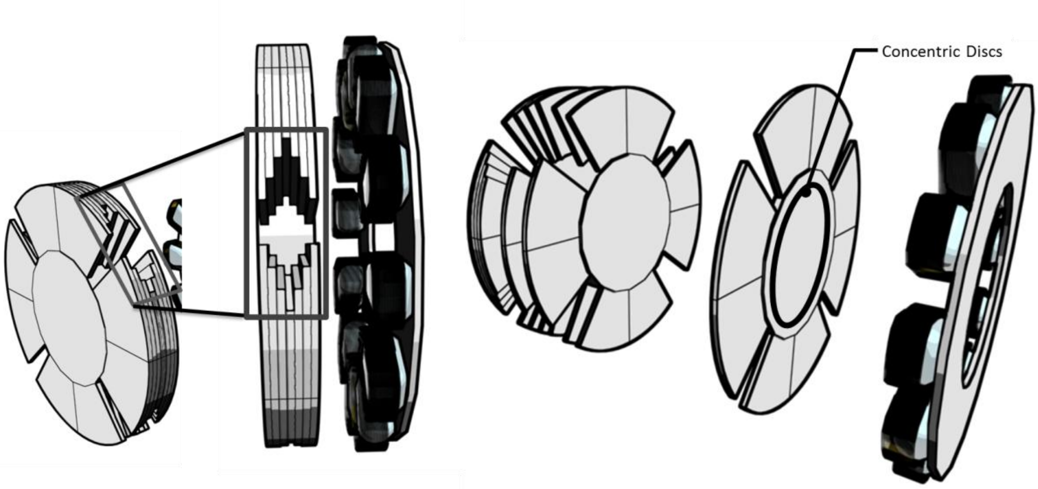

Figure 4.5: Axial flux RSM rotor, construction.

The axial flux RSM should not have eddy currents as it operates synchronously. During start-up however, there might be some eddy currents. If these needed to be reduced concentric discs of each lamination could be cut out, to prevent eddy currents.

This design would offer interesting research areas for optimisation of torque and cost. FEM analysis could be done on which “pattern cut out” should be used, the lamination widths and other factors similar to the design done for the radial RSM [10]. Furthermore interesting configurations like multiple platters of stacked stator/rotor/stator designs could also be researched.

This new design would be particularly useful for electric vehicles of the future that have been discussed, and adapts the radial RSM to an axial design. Axial flux designs are gaining popularity because of their uses for in-wheel motors.

All these insights from the mine shuttle vehicle research show that the RSM would have positive, wide ranging societal impacts. This is particularly due to its unique cost and performance package, which is a significant improvement on the IM. This highlights the significance of future research on the RSM, in industrial applications.

4.5 Summary

This chapter provided the analysis of the two motors and showed that the RSM does indeed offer significant advantages over the IM, in terms of torque production. It also discusses areas for future work, social implications of the work and new developments that arose from the work. The next chapter will conclude and present the future work still to be done.

Chapter 5

Conclusion

The research into the RSM was initiated to see whether a local motor manufacturer could produce a more efficient motor at a lower cost. The research also examined the robustness of the RSM construction and the torque produced, for a specific application (underground mine shuttle) when compared with an IM.

This segment of research was a continuation from the initial design using finite element analysis (FEA) [10]. It sought to confirm the initial design of the RSM as a suitable alternative to the IM in the mine shuttle application. Furthermore, it intended to justify whether further research in this direction will lead to positive results.

5.1 Results and Analysis

From the analysis of each motor's construction (Chapter 2 Motors), the testing performed on each motor (Chapter 3 Motor Testing) and the final analysis of the results (Chapter 4 Analysis), it can be seen that the RSM offers significant advantages over the IM particularly when considering the mine shuttle application.

The measurements confirmed the predictions made in the design simulations and in some cases exceeded the predictions made (Table 5.1). This is evident in the amount of torque produced. The torque produced by the RSM was 13 N.m (3.6%) greater than the IM at the same rated current. The RSM also has the ability to produce 143 % of the torque at 129 % the current of the IM. This ability of the RSM is because of its construction, which prevents the motor from heating up excessively, and thus allows larger currents to be supplied to the motor [15]. This demonstrates the RSM's higher torque density.

Table 5.1: Torque Improvements of the RSM

Motor Type	Torque	Current	Torque Improvement (%)
Induction Motor	355 N.m	93 A (Rated)	
Reluctance Synchronous Motor	369 N.m	93 A	3.9 %
	510 N.m	120 A (129 % Rated)	43.66 %

Based on these results, the research validates that the prototype RSM is a viable alternative to the IM, in the mine shuttle application. This is because the RSM has a robust, cheaper and less complex construction as well as the ability to produce more torque (i.e. higher torque density). This justifies further research into the efficiency of the motor.

5.2 Future Work

Further work on the RSM would include quantifying its efficiency, through the implementation of a vector control system (using a VSD). This would require control systems to be implemented to allow the motor to operate at various torque angles. The setup for this system would also allow a number other control systems to be implemented, like MTC, MRCTC, and MPFC. The vector control theory and d-q modelling for the RSM requires further research to implement these control techniques.

5.3 Conclusion

This research verifies the improvements offered by the initial design and construction. Measurements were taken for both the RSM and the IM in order to evaluate the advantages of each motor. These measurements determined that the RSM was better in niche applications that already use VSDs, as it offered: robust, reliable and cheaper construction with reduced complexity. In addition its ability to produce (43.66 %) more torque (higher torque density) was another advantage. The measurements matched the predictions of the initial FEM design simulations, and showed the effectiveness of FEM for initial prototyping. Future work involves the development of a vector control system that would allow the motor to operate at different torque angles, and quantify the motor's efficiency. The research has the potential for significant benefits for society in terms of reducing pollution, improving industries and developing the next generation of transportation.

Appendix A

Siemens Simoreg DC Master Drive

Setup Configuration

Authors: Lerato Maraba and Mikail Muhammad Aleem Ansari

Created on: 2011-08-10

Contact: 011-717-7259

E-mail: lerato.maraba@wits.ac.za

Genmin Laboratory

A.1 Introduction

This document shows the new configuration of machines 11A and 5A, shown in Figure 1. The machine 11A is a DC shunt motor. It is a Mawdsley DC machine. The motor was originally powered by panel 11A but was recently replaced with a Siemens Simoreg DC master digital converter/drive, shown in Figure 2. The DC motor is mechanically coupled to the synchronous generator 5A. The synchronous generator provides a varying frequency/voltage sinusoidal waveform based on the speed of the DC motor and the supplied field current. Motors 11A and 5A are known on the GEC transformer panel board as ALT 2. This means that it is the second alternate source of power with which it can be run on.

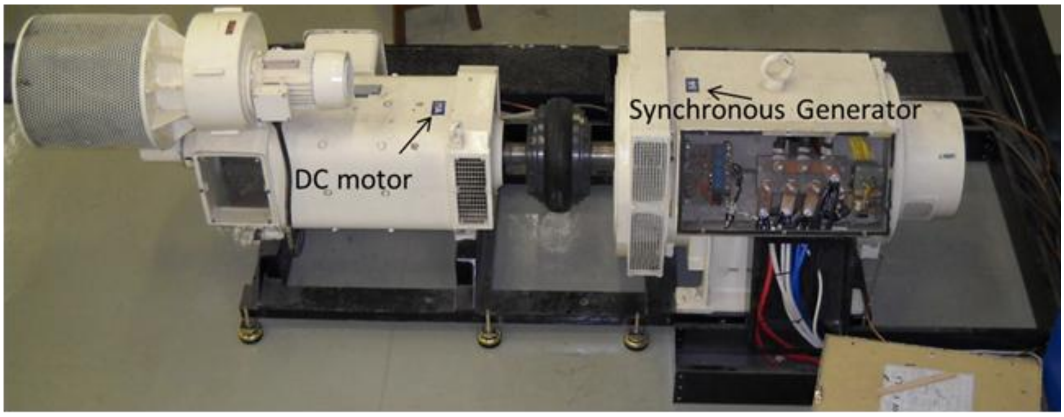

Figure 5.1: DC motor and Synchronous generator set (GENSET)

Figure 5.2: Siemens Simoreg DC master digital converter/drive

A.2 SIEMENS SIMOREG DC MASTER DRIVE

The converter runs the machine digitally. The converter and all the components connected to it will be moved and mounted onto panel board 11A. The circuit breaker configuration is shown in Figure 3.

Figure 5.3: Initial configuration of circuit breakers

Simoreg DC master comes with an operator panel which is portable. This handy operator panel allows us to control the converter from the other end of the lab.

Figure 5.4: Portable operator panel (OP1S)

A.3 Labelling the wires

The labelling of the wires was done to identify where each wire fits in and also to easily connect all wires once it is ready to mount in panel 11A

A.3.1 Bill of Materials

The following items were used to number the wires

Quantity	*Description*
1	Packet of Cable ties
1	Box of Black label holders
1	Box of Cable markers

Figure 5.5: Picture of labelled DC Siemens Drive connecting to Siemens reactor and Siemens 3NE fuses

A.3.2 Numbering List

Number	*Start*	*Colour*	*Stop*
131	3D Simoreg DC Master	yellow	Terminal block 1:1
130	3C Simoreg DC Master	yellow	Terminal block 1:2
311	3W1 Simoreg DC Master	yellow	Siemens AC Reactor 2
301	3U1 Simoreg DC Master	yellow	Circuit breaker 1:2 bottom
51	5U1 Simoreg DC Master	yellow	Circuit breaker 2:2 bottom
52	5W1 Simoreg DC Master	yellow	Circuit breaker 2:1 bottom
108	108 Simoreg DC Master	brown	Reset switch

107	107 Simoreg DC Master	brown	E-stop switch
38	38 Simoreg DC Master	brown	start button
37	37 Simoreg DC Master	brown	switch on button
341	34 Simoreg DC Master	brown	start button
342	34 Simoreg DC Master	brown	switch on button
106	106 Simoreg DC Master	brown	Reset switch
116	106 Simoreg DC Master	brown	E-stop switch
41	Simoreg DC Master fan 4U1	yellow	Circuit breaker 3:1 bottom
42	Simoreg DC Master fan 4V1	yellow	Circuit breaker 3:2 bottom
43	Simoreg DC Master fan 4W1	yellow	Circuit breaker 3:3 bottom
31	Circuit breaker 3:1 bottom	yellow	terminal block 1:5 top
32	Circuit breaker 3:2 bottom	yellow	terminal block 1:4 top
33	Circuit breaker 3:3 bottom	yellow	terminal block 1:3 top
91	Circuit breaker 3:1 top	yellow	Circuit breaker 0:1 bottom
92	Circuit breaker 3:2 top	yellow	Circuit breaker 0:3 bottom
93	Circuit breaker 3:3 top	yellow	Circuit breaker 0:2 bottom
21	Circuit breaker 2:1 top	yellow	Circuit breaker 0:2 bottom
22	Circuit breaker 2:2 top	yellow	Circuit breaker 0:1 bottom
321	Circuit breaker 1:3 bottom	yellow	Siemens AC Reactor 1
11	Circuit breaker 1:3 top	yellow	Fuse 6 top
12	Circuit breaker 1:2 top	yellow	Fuse 5 top
5	Fuse 5 bottom	black	alt 2 Siemens
6	Fuse 6 bottom	black	alt 2 Siemens
1	terminal block 1:1 bottom	red	alt 2 Siemens
2	terminal block 1:2 bottom	black	alt 2 Siemens
3	terminal block 1:3 bottom	blue	alt 2 Siemens
4	terminal block 1:4 bottom	white	alt 2 Siemens
0	terminal block 1:5 bottom	red	alt 2 Siemens
7	terminal block 1:6 bottom	blue	alt 2 Siemens
8	terminal block 1:7 bottom	black	alt 2 Siemens

A.3.3 Quantifying the quality of supply

This Genset is expected to provide balanced 3-phase waveforms. To make certain that these voltage waveforms were balanced, the Genset supply was tested. IEC/SABS standards [16] were used to quantify the extent of supply imbalance.

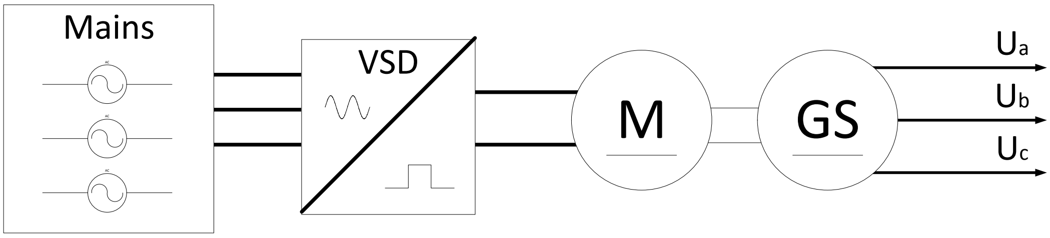

Figure 5.6: Genset circuit diagram

The percentage unbalance of Genset outputs (U_a, U_b, and Uc) in the circuit (Figure 3.2) is evaluated according to the IEC/SABS standard [16]. This standard states that in an unbalanced system the following components are present, positive sequence components (U_1), Negative sequence (U_2) components and/or Zero sequence components (U_0).

By categorising the extent of negative sequence components in the system relative to positive sequence, the amount of unbalance in the supply can be quantified. The Negative sequence (U_2) ratio (u_2) is expressed as:

$$u_2 = \frac{U_2}{U_1} \times 100 = \frac{negative\ sequence}{positive\ sequence} \times 100 \quad (1)$$

$$u_2 = \sqrt{\frac{1 - \sqrt{3 - 6\beta}}{1 + \sqrt{3 - 6\beta}}} \times 100$$

$$with\ \beta = \frac{U_{ab\ fund}^4 + U_{bc\ fund}^4 + U_{ca}^4}{\left(U_{ab\ fund}^2 + U_{bc\ fund}^2 + U_{ca}^2\right)^2} \quad (2)$$

$$with\ U_{ab} = 441.30, U_{bc} = 441.00, U_{ca} = 441.30$$

$$the\ negative\ sequence\ ratio\ is\ calculated\ to\ be: \quad (3)$$

$$u_2 = 0.046\%$$

The negative sequence is determined to be less than 0.05%. As many measurement instruments have errors larger than this (for example the torque sensor has a 1%

error), this 0.05% error can be considered to be negligible (falling within the error margin) and the supply can be considered to be balanced.

A.3.4 Implementation issues

During implementation of the required changes a number of issues came up. These included the following:

- Switches, the drive required DC switches. An AC switch was connected initially, which requires some capacitance to complete the switching operation. This did not achieve the desired operation.
- The drive was wired to have two enable signals, one which is start/shutdown button and one which is an enable button. This was to ensure another layer of safety however it increased the complexity of the system as multiple circuit breakers were already in place to ensure safety.
- Currently the enable button is "hardwired", however this situation should be re-evaluated in other systems.
- The reset button is removed and the reset action is controlled by removing the estop, removing the start and pushing the start in again.
- Switch connectors, the Lugs used to connect to the switches sometimes did not make complete contact. This problem was solved by connecting the switches with multi-strand wire.
- Wiring, the wiring was directly connected to the mains (this was for quick prototyping) however when the mains was switched on some components went live. A secondary layer of protection should be added (a second circuit breaker), as the main switch is sometimes used to power other projects. The circuit breaker has been added on.

- Fuses are connected between mains and circuit breaker 1 (CB1) which are not on the diagram.
- Manual Field weakening is done by changing the maximum and minimum field current parameters.
- Automatic field weakening cannot be done without the tachometer.
- The tachometer has been wired in but is not shown in the diagram below.
- The tachometer is necessary to do field weakening and automatic speed control.
- The connection from the tachometer to the drive was without a shielded cable, and the cable was running together with the power cables for the drive. This can cause some issues in terms of inductive effects on the speed measurement and cause errors in the field control.
- It is recommended that this document always be supplied together with the datasheet.
- For setup of the drive, the datasheet is quite extensive. The most important section in the datasheet is the start-up section (section/chapter 8), please read this section carefully.
- Furthermore the functional diagrams are recommended.
- Another important section is the error lists. It is recommended the error command be entered using the find function in pdf readers.
- An error can be reset by hitting reset on the main scree of the OPS1 control panel, or hitting P on the drive display.

A.4 Implementation

Current Situation (3/8/2010)

The system has been wired so that it can be controlled by the enclosure front panel (with the potentiometer and the switches) Figure 6a, as well as with the OP1S control panel (with the LCD display), Figure 6b. Currently the "reset" labelled button will toggle between control techniques, Figure 6b.

The potentiometer rating at 8 is classified as 100 % speed which is 1750 for the generator. Note the potentiometer is slightly faulty in its range, as it goes from 0 to 70% not to 100%; this has been compensated for by the drive. An overview of the drive setup is shown in Figure 7a and the drive enclosure is shown in Figure 7b.

A

B

Figure 5.7: Enclosure front panel controls b) Op1s Operator Panel shown with "reset" (remote) switch.

A

B

Figure 5.8: a) Overview of drive connections b) Drive enclosure

A.4.1 Tasks to still be completed:

- Update diagrams.
- Use shielded cable for taco and implement field optimization run.
- Sort out reset switch.
- Check out remote estop connections for the synchronous generator

The total lab setup is shown in Figure 8.

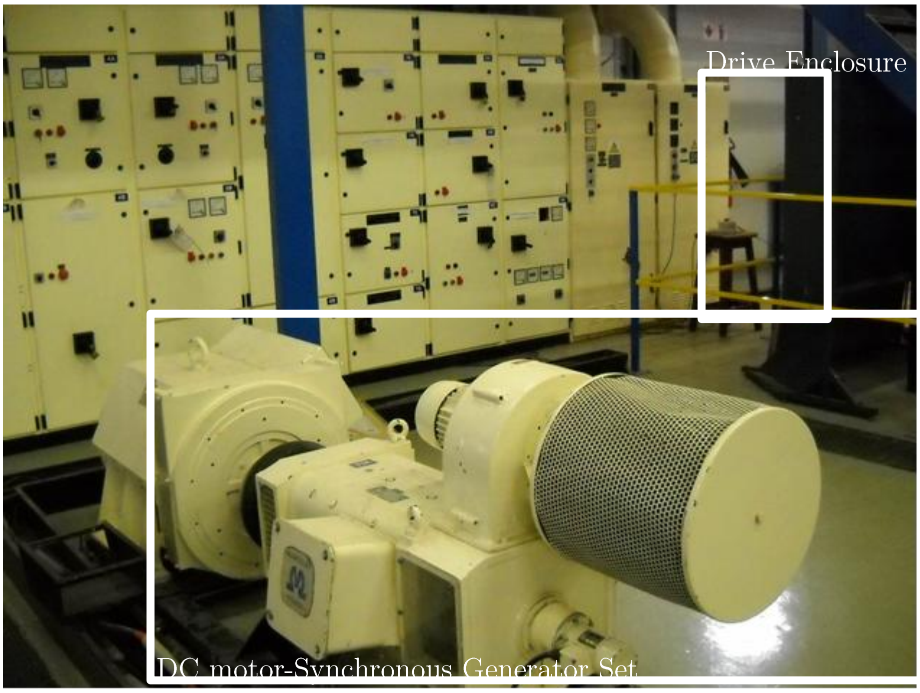

Figure 5.9: a) Complete laboratory setup.

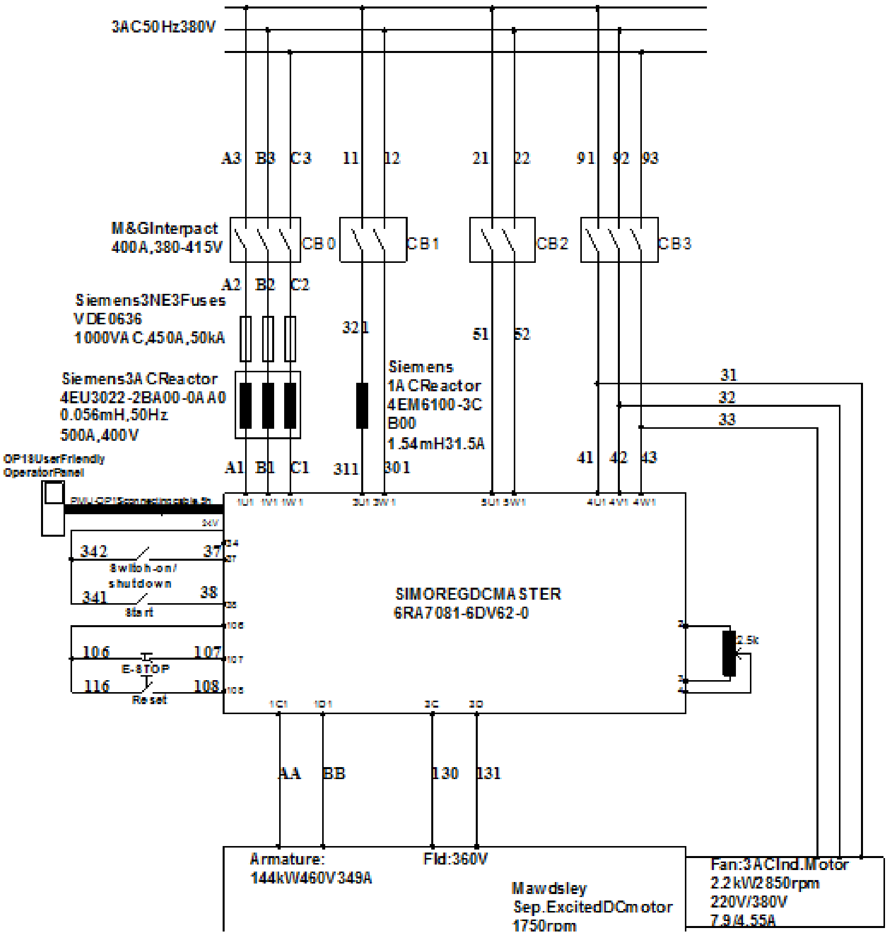

Figure 5.10: Drive connection diagrams

Appendix B

Measurement Transducers Analysis

B.1 Introduction

This document shows the analysis of the transducers in the measurement system, so that the accuracy and confidence in the measurements can be determined. The system was composed of transducers like Differential probes, the torque transducer, the encoder and the current clamp.

B.2 Transducers

B.2.1 Differential Voltage Probe

This GE Elditest 8115 Differential probe was used to get the voltage measurements of the machine to the dSpace real-time interface. This differential probe had an error of 3%.

B.2.2 Current Clamp

The current clamp used, was the Fluke 80i-500s. This clamp had an error of 5% at rated current 93 A. This 5% error equates to 4.65 A, for the measurement at rated current.

B.2.3 Torque transducer

The Magtrol M420 torque transducer had a range of 0 to 2000 N.m error of 0.1 % FSD (full scale deflection). This translated to a 2 N.m absolute error.

As the torque generated by the RSM at rated current was 369 N.m, this measurement would have 0.5% error margin which is quite reasonable. At 129 % of rated current, 510 N.m of torque was generated, and this would have had a 0.4% error margin.

B.2.4 Encoder

The Leine & Linde RHI 503 incremental encoder was used to measure the position. The encoder had a resolution of 500 pulses per revolution. The dividing accuracy is ± 50 el° [25]. This means that the maximum error is 50/500 mechanical degrees, which is 0.1° mechanical error. This equates to 0.1/360*100%, 0.028%.

B.2.5 dSpace

The dSpace break out box also has errors associated with the ADC. The 4 x 12 bit ADC has ± 5 mV offset error and ± 0.5 % gain error on a ± 10 V input range.

B.3 Measurement System

It is important to evaluate the entire measurement system, from the input true value to the output displayed value [26].

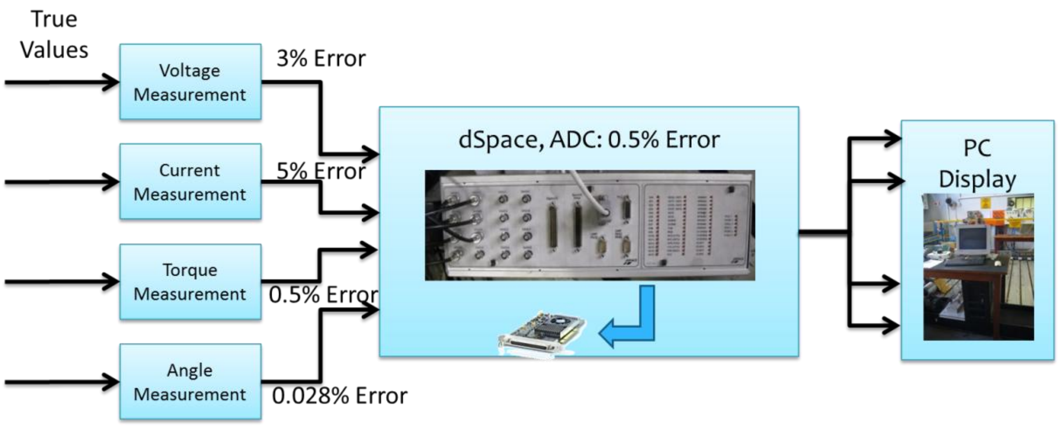

Figure 5.11: Error analysis of measurement system, adapted from [26]

Overall, the errors on the final values that are displayed would be (according to [26]):

- Voltage: 3%*0.5%=0.015%
- Current: 5%*0.5%=0.025%
- Torque: 0.5%*0.5%=0.0025%
- Angle/Position: 0.28%*0.5%=0.00014%

B.4 Discussion

The error analysis of the measurement system shows that the Torque and Encoder measurements are more accurate when compared with the voltage and current measurements. This means that there should be a higher degree of confidence in the efficiency calculations based on the torque and encoder measurements as opposed to the classic current and voltage measurements that were conducted. Furthermore, the error in the voltage measurements negates any measure of unbalance that the supply system may have which was calculated in A.3.3 Quantifying the quality of supply in Appendix A.

B.5 Summary

The measurement system was analysed and showed that the torque and encoder measurements are substantially more accurate than the voltage and current measurements. This justifies the use of these transducers in determining motor performance.

References

[1] J. Wander, V. Byrd, and J. Parker, "Initial disturbance accommodating control system analysis for prototype electromechanical Space Shuttle steering actuator," in *American Control Conference, 1995. Proceedings of the*, 1995, pp. 3961-3964.

[2] R. Valentine, *Motor Contol Electronics Handbook*, 1st ed., Onken B, Ed. United States: McGraw-Hill, 1998.

[3] P. Waide and C. U. Brunner, "Energy-Efficiency Policy Opportunities for Electric Motor-Driven Systems," International Energy Agency, Paris, France, Working Paper 2011.

[4] Eskom Demand Side Management. (2011, July) Eskom Integrated Demand Management. [Online]. http://www.eskomidm.co.za/library#GuidelineDocs

[5] A De Almeida, F. Ferreira, J. Fong, and P. Fonseca, "EuP Lot 11 Motors, Ecodesign Assessment of Energy Using Products," ISR-University of Coimbra, February 2008.

[6] A. Vagati, "The synchronous reluctance solution: a new alternative in AC drives," in *Industrial Electronics, Control and Instrumentation*, vol. 1, 1994, pp. 1-13.

[7] (2010, February) Trans Vaal Electric (TVE) Web site. [Online]. http://www.transelectric.co.za/

[8] R.E. Betz, R. Lagerquist, M. Jovanovic, T.J.E. Miller, and R.H. Middleton, "Control of synchronous reluctance machines," *Industry Applications, IEEE Transactions on*, vol. 29, no.6, pp. 1110-1122, Nov/Dec 1993.

[9] J.G. Wright and W.A. Cronje, "The Electromagnetic and mechanical design of a reluctance synchronous machine rotor using the finite element method," in *Southern African Universities Power Engineering Conference*, Johannesburg, 2010, pp. 48-54.

[10] J G Wright, "Design of a Synchronous Reluctance Motor for traction drive application using the finite element method," University of the Witwatersrand, Johannesburg, 2010.

[11] Department of Energy Handbook of Electrical Science. (2010, March) Knowledge Publications. [Online]. http://knowledgepublications.com/doe/images/DOE_Electrical_Science_Squirrel-Cage_Induction_Rotor.gif

[12] R. E. Doherty and O. E. Shirley, "Reactance of Synchronous Machines and its Applications," *American Institute of Electrical Engineers, Transactions of the*, vol. XXXVII, no.2, pp. 1209-1340, July 1918.

[13] P. L. Alger and H. W Samson, "Shaft Currents in Electric Machines," *American Institute of Electrical Engineers, Transactions of the*, vol. XLIII, no., pp. 235-245, Jan 1924.

[14] R. E. Doherty and R. H. Park, "Mechanical Force Between Electric Circuits," *American Institute of Electrical Engineers, Transactions of the*, vol. XLV, no., pp. 240-25, Jan 1926.

[15] A. Cavagnino, M. Pastorelli, D. Staton, and A. Vagati A. Boglietti, "Thermal analysis of induction and synchronous reluctance motors," in *IEEE International Conference on Electric Machines and Drives,* vol. 1, May 2005, pp. 1592 – 1597.

[16] IEC, SANS 61000-4-30:2009 Electromagnetic compatibility (EMC) Part 4-30: Testing and measurement techniques — Power quality measurement methods, 2009.

[17] P.C. Sen, *Principles of electric machines and power electronics*, 2nd ed. Ontario, Canada: John Wiley & Sons, 1997.

[18] M.G. Say, *Alternating Current Machines*, 4th ed. London, Great Britain: Pitman Publishing Limited, 1976.

[19] IEEE Power Engineering Society, IEEE Standard Test Procedure for Polyphase Induction Motors and Generators, 2 November 2004.

[20] IEC, Rotating electrical machines- Standard methods for determining losses and efficiency from tests, 2007, pg 53.

[21] R.E. Betz, M. Jovanovic, R. Lagerquist, and T.J.E. Miller, "Aspects of the control of synchronous reluctance machines including saturation and iron losses," in *Industry Applications Society Annual Meeting, 1992., Conference Record of the 1992 IEEE*, vol. 1, 1992, pp. 456-463.

[22] J. Haataja, "A comparative performance study of four-pole induction motors and synchronous reluctance motors in variable speed drives," Lappeenranta University of Technology, Lappeenranta, Finland, Ph.D. dissertation June 2003.

[23] R.E. Betz, "Theoretical aspects of control of synchronous reluctance machines," *Electric Power Applications, IEE Proceedings B*, vol. 139, no.4, pp. 355-364, Jul 1992.

[24] A. Consoli, C. Cavallaro, G. Scarcella, and A. Testa, "Sensorless Torque Control of Syncrel Motor Drives," *Power Electronics, IEEE Transactions on*,

vol. 15, no. 1, pp. 28-35, Jan 2000.

[25] Leine & Linde. (2011, Oct.) Leine Linde. [Online]. http://www.leinelinde.com/PageFiles/2266/technical_info_eng.pdf

[26] John P. Bentley, *Principles of Measurement Systems*, Fourth Edition ed. Essex, England: Pearson Education Limited, 2005.